RESEARCH ARTICLE

Key Points:
- Higher TEX_{86}-based temperatures than SST-$U^{k'}_{37}$ by 5.6 degree Celcius when using global calibrations
- Modeled temperature proxies in ROMS tested for present, LGM, and Heinrich Stadial
- New TEX_{86} regional calibration to reconstruct present and past annual mean SSTs off Portugal

Sea surface temperature reconstructions over the last 70 kyr off Portugal: Biomarker data and regional modeling

Sophie Darfeuil[1], Guillemette Ménot[1,2], Xavier Giraud[1], Frauke Rostek[1], Kazuyo Tachikawa[1], Marta Garcia[1], and Édouard Bard[1]

[1]Aix-Marseille Université, CNRS, IRD, Collège de France, CEREGE UM34, Aix-en-Provence, France, [2]Now at Laboratoire de géologie de Lyon, ENS de Lyon, Université de Lyon, CNRS, Lyon, France

Abstract This study aims at providing robust temperature reconstructions for a key oceanographic setting in the North Atlantic and at understanding the nature of the temperature signal recorded by the two biomarkers $U^{k'}_{37}$ and TEX_{86}, considering season and depth of production. To do so, high-resolution signals of $U^{k'}_{37}$ and TEX_{86} are determined for the last 70 kyr for core MD95-2042, located off Portugal. Signals of $U^{k'}_{37}$ and TEX_{86} present a tight correlation, demonstrating a dominant temperature effect. $U^{k'}_{37}$ signals correspond well to the annual mean sea surface temperature (SST), whereas TEX^{H}_{86}-derived temperatures are 5.6°C higher, which is unrealistically warm for this area. Unsuitable TEX_{86} global linear calibrations on the Iberian Margin may suggest a possible occurrence of archaeal communities with specific temperature response. To assess the impact of different season or depth of production of the biomarkers on the recorded temperature in the sediment, modeled temperature proxies (Tproxies) are introduced in a Regional Oceanic Modeling System and tested for different seasons (annual/summer/winter) and depths (surface and 0–200 m) of production for three climate modes (Present Day (PD), Last Glacial Maximum (LGM), and Heinrich Stadials (HS)). Similar temperature amplitudes between climate modes are found at MD95-2042 core site for observations, for both biomarkers, and for modeled annual surface production Tproxy: 5.5–7°C for ΔT(PD-LGM) and 3–4°C for ΔT(LGM-HS). Therefore, we propose a new TEX^{H}_{86} regional calibration to reconstruct present and past annual mean SSTs on the Iberian Margin.

1. Introduction

The Iberian Margin (36–44°N; 8–12°W) is a key area for the reconstruction of past sea surface temperatures (SSTs). These records are often cited as the reference signals for North Atlantic climate variations and represent important information for the study of climate system dynamics between high and middle latitudes in the Northern Hemisphere [*Bard et al.*, 1987, 2000; *Shackleton et al.*, 2000; *Martrat et al.*, 2007]. During Heinrich events [*Heinrich*, 1988; *Bond et al.*, 1992; *Bond and Lotti*, 1995], the Iberian Margin's distal position outside of the main belt of ice rafting prevents the sedimentary SST record from disturbance [*Bard et al.*, 2000; *Pailler and Bard*, 2002]. Moreover, high sedimentation rates make this margin particularly well suited for studying abrupt climatic variability of the last glacial/interglacial cycles with adequate resolution [*Bard et al.*, 1987; *Cayre et al.*, 1999; *Bard et al.*, 2000; *Pailler and Bard*, 2002; *Moreno et al.*, 2002; *Thouveny et al.*, 2004; *Martrat et al.*, 2007; *Voelker and de Abreu*, 2011; *Martrat et al.*, 2014].

Several proxies are commonly used to reconstruct SST, among which are organic biomarkers. The $U^{k'}_{37}$ index (C_{37} ketone unsaturation ratio) is based on the relative abundance of di-unsaturated ($C_{37:2}$) and tri-unsaturated ($C_{37:3}$) alkenones, whereby the proportion of $C_{37:3}$ alkenone decreases with increasing water temperature [*Brassell et al.*, 1986; *Prahl and Wakeham*, 1987]. The $U^{k'}_{37}$ is calculated according to *Prahl and Wakeham* [1987]:

$$U^{k'}_{37} = \frac{[C_{37:2}]}{[C_{37:2}] + [C_{37:3}]} \tag{1}$$

Alkenones are synthesized by a small group of haptophyte algae, mainly the coccolithophore *Emiliania huxleyi* and related species growing in the ocean's surface waters [*de Leeuw et al.*, 1980; *Volkman et al.*, 1980; *Marlowe et al.*, 1984]. Culture and core top studies have shown that the $U^{k'}_{37}$ index correlates well and linearly with annual mean SST [*Prahl and Wakeham*, 1987; *Prahl et al.*, 1988; *Müller et al.*, 1998; *Conte et al.*, 2006].

A more recently developed SST proxy, the TEX$_{86}$ index [*Schouten et al.*, 2002], is based on the relative abundance of isoprenoid glycerol dialkyl glycerol tetraethers (GDGTs) that are produced by marine Thaumarchaeota (formerly Group 1 Crenarchaeota) [*Sinninghe Damsté et al.*, 2002; *Schouten et al.*, 2013b, and references cited therein], a major group of ammonia-oxidizing [*Konneke et al.*, 2005; *Wuchter et al.*, 2006; *Ingalls et al.*, 2006] prokaryotes in today's ocean [*Karner et al.*, 2001; *Herndl et al.*, 2005]. The proportion of cyclic moieties in GDGTs increases with rising growth temperature in mesocosm experiments [*Wuchter et al.*, 2004; *Schouten et al.*, 2007], and in worldwide data sets of core tops it is correlated to mean annual sea surface temperature [*Schouten et al.*, 2002; *Kim et al.*, 2008, 2010]. The TEX$_{86}$ ratio is calculated according to *Schouten et al.* [2002]:

$$\text{TEX}_{86} = \frac{[\text{GDGT}-2]+[\text{GDGT}-3]+[\text{GDGT}-4']}{[\text{GDGT}-1]+[\text{GDGT}-2]+[\text{GDGT}-3]+[\text{GDGT}-4']} \qquad (2)$$

where numbers refer to the number of cyclopentane moieties in GDGTs and GDGT-4' represents the crenarchaeol isomer with one additional cyclopentane moiety. More recently, *Kim et al.* [2010] proposed updated indices which present higher global correlation to annual mean SST and which are calculated as follows:

$$\text{For } T \leq 15°C: \qquad \text{TEX}_{86}^{L} = \log\left(\frac{[\text{GDGT}-2]}{[\text{GDGT}-1]+[\text{GDGT}-2]+[\text{GDGT}-3]}\right) \qquad (3)$$

$$\text{For } T \geq 15°C: \qquad \text{TEX}_{86}^{H} = \log(\text{TEX}_{86}) \qquad (4)$$

Although both U$_{37}^{k'}$ and TEX$_{86}$ organic proxies are calibrated against annual mean SST using surface sediments, some studies report biases toward a given season or greater water depths, which leads to differences in the temperature recorded by both biomarkers in various oceanographic settings [*Huguet et al.*, 2006b; *Castañeda et al.*, 2010; *Leider et al.*, 2010; *Huguet et al.*, 2011; *Shintani et al.*, 2011; *Jia et al.*, 2012; *Kim et al.*, 2012; *McClymont et al.*, 2012; *Nakanishi et al.*, 2012a; *Seki et al.*, 2012; *Studer et al.*, 2012; *Grauel et al.*, 2013; *Li et al.*, 2013; *Lopes dos Santos et al.*, 2013; *Nieto-Moreno et al.*, 2013; *Shaari et al.*, 2013; *Turich et al.*, 2013; *Zhang et al.*, 2013; *O'Brien et al.*, 2014; *Ho and Laepple*, 2015]. The Iberian Margin—a seasonally, spatially, and climatically contrasted area—is an ideal place to study potential differences between SST proxies and to better comprehend the behavior of alkenone and GDGT biomarkers.

The main goals of this study are to provide the paleoclimatic community with robust temperature reconstructions for a key oceanographic setting in the North Atlantic and to understand the nature of the temperature signal actually recorded by both biomarkers U$_{37}^{k'}$ and TEX$_{86}$, especially in terms of season and depth of production. To do so, we first present our reference records, i.e., high-resolution U$_{37}^{k'}$- and TEX$_{86}$-derived SST reconstructions for the last 70 kyr for core MD95-2042. To explain the observed temperature differences between biomarkers, possible scenarios of production are mentioned and tested in parallel by modeling. We conducted regional ocean simulations for three climate modes (Present Day, Last Glacial Maximum, and Heinrich Stadial), which are typical and contrasted in terms of oceanographic conditions and biomarker temperature records. A new tool, the modeled temperature proxy (Tproxy), is used to test different seasons and depths of production and to evaluate/quantify the resulting temperature record on the seafloor for all three climate modes. Biomarker results are confronted with the modeled Tproxies, contributing to a better understanding of the temperature signal's origin.

2. Possible Biases for Organic SST Proxies

Many factors may bias U$_{37}^{k'}$ temperature reconstructions, including Coccolithophorid physiological growth factors such as the availability of nutrients and light [*Epstein et al.*, 1998; *Versteegh et al.*, 2001; *Prahl et al.*, 2003], the lateral transport of alkenones in shallow depth environments [*Benthien and Müller*, 2000; *Ohkouchi et al.*, 2002; *Rühlemann and Butzin*, 2006; *Mollenhauer et al.*, 2006, 2007], differences in species composition [*Volkman et al.*, 1995; *Conte et al.*, 1998], production at greater depth in the mixed layer [*Ternois et al.*, 1996, 1997; *Prahl et al.*, 2001, 2005], or seasonal blooming haptophytes [*Prahl et al.*, 1993, 2001, 2010; *Sikes et al.*, 1997; *Ternois et al.*, 2000; *Leider et al.*, 2010; *Schneider et al.*, 2010; *Sicre et al.*, 2013]. Even if some studies show no effect of alkenone degradation in the water column or during early sediment diagenesis on the U$_{37}^{k'}$ signal [*Prahl et al.*, 1989, 1993; *Sawada et al.*, 1998; *Goni et al.*, 2004], preferential degradation of the C$_{37:3}$

alkenone may occur, leading to a warm bias in the final sedimentary $U_{37}^{k'}$ record [*Sun and Wakeham*, 1994; *Gong and Hollander*, 1999; *Rontani et al.*, 2006, 2007, 2008, 2009; *Rontani and Wakeham*, 2008; *Kim et al.*, 2009; *Zabeti et al.*, 2010; *Prahl et al.*, 2010; *Turich et al.*, 2013].

Deviations of TEX$_{86}$-derived temperatures from annual mean SSTs have often been explained by differences in the growth season of Thaumarchaeota [*Castañeda et al.*, 2010; *Leider et al.*, 2010; *Huguet et al.*, 2011; *Shintani et al.*, 2011; *Grauel et al.*, 2013; *Lopes dos Santos et al.*, 2013; *Nieto-Moreno et al.*, 2013; *Lü et al.*, 2014] or by its production below the mixed layer (especially in upwelling areas) [*Huguet et al.*, 2007; *Lee et al.*, 2008; *Lopes dos Santos et al.*, 2010; *Rommerskirchen et al.*, 2011; *Jia et al.*, 2012; *Kim et al.*, 2012; *McClymont et al.*, 2012; *Nakanishi et al.*, 2012a, 2012b; *Seki et al.*, 2012; *Li et al.*, 2013; *Shaari et al.*, 2013; *Smith et al.*, 2013; *Hernández-Sánchez et al.*, 2014; *Ho and Laepple*, 2015]. Oxydation and diagenesis [*Schouten et al.*, 2004; *Huguet et al.*, 2009; *Kim et al.*, 2009; *Bogus et al.*, 2012; *Turich et al.*, 2013], or advection, seem to affect TEX$_{86}$ less than the $U_{37}^{k'}$ index, but selective degradation of Crenarchaeol regioisomer compared to other GDGTs during lateral advection may significantly influence the initial TEX$_{86}$ index [*Mollenhauer et al.*, 2008; *Shah et al.*, 2008].

In addition, water column Archaea or benthic Archaea living in marine sediments can constitute a potential source of isoprenoidal GDGTs that may affect the TEX$_{86}$ signal, with a positive offset of up to +3°C in regions within the oxygen minimum zone [*Lipp et al.*, 2008; *Shah et al.*, 2008; *Lipp and Hinrichs*, 2009; *Liu et al.*, 2011; *Weijers et al.*, 2011; *Lengger et al.*, 2012, 2013, 2014]. High nutrient concentrations and different species contributions (pelagic Euryarchaeota) are also mentioned as possible sources of bias in upwelling areas [*Turich et al.*, 2007]. Euryarchaeota contribution (relative to Thaumarchaeota contribution) to the sedimentary GDGT pool in diverse oceanic settings has recently been confirmed as a possible significant bias for TEX$_{86}$-based temperature reconstructions [*Lincoln et al.*, 2014]. Furthermore, the seasonal upwelling area off Mauritania showed that the inaccuracy of existing TEX-temperature transfer functions may be due to different communities/metabolisms of Archaea dwelling in the subsurface in this specific oceanic province [*Basse et al.*, 2014; *Mollenhauer et al.*, 2015]. Moreover, Thaumarchaeota thriving in deepwater masses of the Mediterranean Sea (>1000 m) contribute to a warm bias on TEX$_{86}$ temperatures and are likely to have a different iGDGT distribution response to in situ temperature than surface-dwelling Archaea, but one which unexpectedly still correlates with SST [*Kim et al.*, 2015].

Finally, GDGTs may derive from land soil organic matter affecting the TEX$_{86}$ record in marine settings in the case of large terrestrial contributions [*Weijers et al.*, 2006], which can be determined by measuring the branched and isoprenoid tetraether (BIT) index, a ratio between terrestrial (branched GDGTs) and marine GDGTs (Crenarchaeol) [*Hopmans et al.*, 2004].

3. Materials and Methods

3.1. Study Area Present and Past Surface Hydrography and Core MD95-2042

The Iberian Margin, now under the influence of the North Atlantic subtropical gyre via two branches—the Portugal and the Azores Currents (Figure 1a1)—has a contrasted seasonal hydrography with a strong coastal-offshore gradient in terms of temperatures and surface currents (Figures 1a2 and 1a3). The area is characterized by a seasonal upwelling which occurs mostly during late spring/summer and which is associated with higher primary productivity and colder temperatures along the coast [*Fiuza et al.*, 1982; *Fiuza*, 1984; *Mazé et al.*, 1997; *Fiuza et al.*, 1998; *Sanchez and Relvas*, 2003; *Navarro and Ruiz*, 2006] (Figure 1a3). In winter, a poleward flow prevails along the coast: the Iberian Poleward Current (IPC), derived mainly from the geostrophic adjustment of the density gradients near the continental slope [*Peliz et al.*, 2003, 2005] (Figure 1a2).

Despite the generally colder climate of the last glacial period, seasonal and spatial patterns were preserved, with a comparable surface hydrology relative to that of the present day and with a more intense seasonal upwelling [*Voelker and de Abreu*, 2011, and references cited therein]. However, during Heinrich Stadials [*Heinrich*, 1988; *Bond et al.*, 1992; *Bond and Lotti*, 1995], the polar front reached the south of the Iberian Margin [*Bard et al.*, 1987; *Eynaud et al.*, 2009], leading to a potential cessation of the upwelling [*Pailler and Bard*, 2002] and a circulation pattern similar to modern winter conditions [*Eynaud et al.*, 2009].

Core MD95-2042 (37°45'N, 10°10'W, 3146 m water depth) (Figure 1) is 3140 cm long, covers the last glacial cycle, and consists mainly of calcareous silty clay [*Bassinot and Labeyrie*, 1996]. The core was collected on
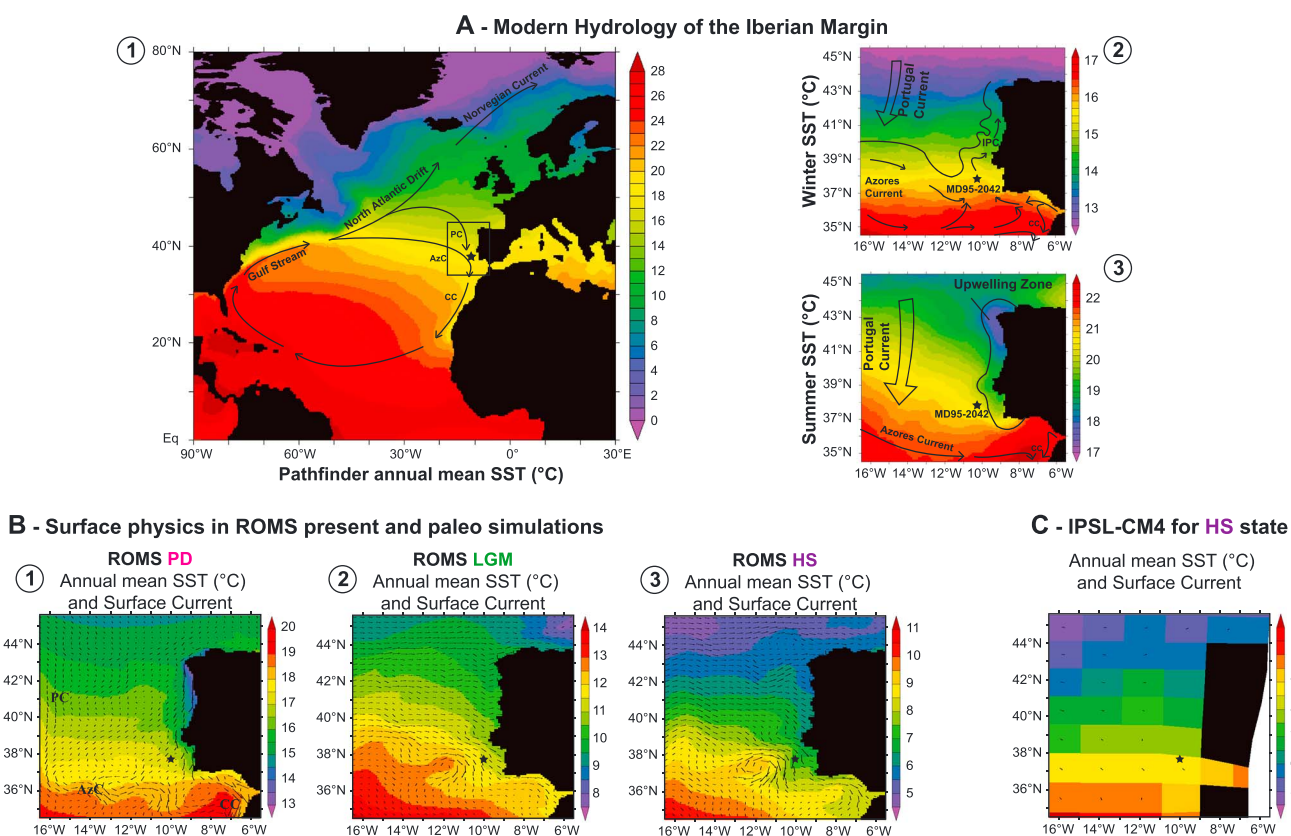
Figure 1. (a) Location and modern hydrology of the studied area: the Iberian Margin. The colored gradient represents Pathfinder SST climatology (9 km resolution) [*Armstrong and Vazquez-Cuervo*, 2001] interpolated on a ROMS grid for the North Atlantic Ocean (1) and off Portugal during winter (2) and during summer (3). Black arrows highlight modern surface circulation patterns, and the black stars represent MD95-2042 core site. PC = Portugal Current; AzC = Azores Current, CC = Canary Current, and IPC = Iberian Poleward Current. (b) Simulated surface physics by ROMS (mean of year 116 to year 125) in the Iberian Margin domain: annual mean SST (colored scales) and annual mean surface currents (arrows) for Present Day (1), Last Glacial Maximum (2), and Heinrich Stadials (3). (c) IPSL-CM4 FWF annual mean SST and surface currents (arrows) on the Iberian Margin domain as inputs for ROMS Heinrich Stadial simulation.

an almost flat continental rise (slope <2%), ~150 km away from the modern coastline, downstream of the Tagus, Setubal, and Sado canyons, and upstream of the Tagus abyssal plain. The site is directly below the pathway of the Iberian Poleward Current (IPC), a branch of the Azores Current, in winter [*Peliz et al.*, 2005], and during summer it is located at the edge of the upwelling area and is currently fed by upwelling filaments developing from Cape Roca to Cape Saõ Vicente [*Fiuza*, 1984] (Figure 1). A new, homogenized chronology for this core is proposed, based on XRF-%CaCO$_3$ tuned on Chinese speleothem δ^{18}O records (see Text S1 in the supporting information).

3.2. $U_{37}^{k'}$ and TEX$_{86}$ Analyses

Core MD95-2042 was sampled every 5 cm, equivalent to an average time resolution of 260 years (Text S4). The 401 lyophilized samples covering the last 70 kyr underwent lipid extraction with the accelerated solvent extraction method (ASE 200, Dionex), following the procedure described in *Pailler and Bard* [2002] (Text S5). The total lipid extracts (TLEs) were subdivided into two identical aliquots, for alkenone analysis and for subsequent purification before GDGT analysis.

Gas chromatography analysis of alkenones was performed by means of a *Thermo Scientific Trace GC* equipped with a flame ionization detector, using analytical conditions similar to those described by *Sonzogni et al.* [1997] (Text S6). The $U_{37}^{k'}$ was calculated according to *Prahl and Wakeham* [1987] (equation (1)).

The precision of our analytical procedures for the SST determination has been assessed in the framework of the international alkenone intercomparison [*Rosell-Melé et al.*, 2001]. Forty replicates of the core catcher

sample of MD95-2042 gave a mean $U^{k'}_{37}$ of 0.557 ± 0.010 ($15.25 \pm 0.26°C$) and a mean alkenone C_{37tot} concentration of 184 ± 27 ng/g sediment. These 40 replicates presented no significant deviation over the period 2012 to 2014, exceeding the data set acquisition of the present paper. Finally, the lack of systematic shifts between the new high-resolution alkenone record and that measured in 1998 [*Pailler and Bard*, 2002], for both standard sediment and downcore samples, rules out a significant laboratory degradation of alkenones in core MD95-2042 over the last 15 years and allows to propose a new high-resolution alkenone record (Text S6).

Prior to GDGT analysis, the total lipid extracts (TLEs) were separated into apolar and polar fractions (containing GDGTs), using the Gilson GX-271 ASPEC^{TM} system controlled by TRILUTION^{TM}LH software [*Sanchi et al.*, 2013]. Polar fractions were analyzed by high-performance liquid chromatography/atmospheric pressure chemical ionization mass spectrometry, following an analytical procedure similar to the one described by *Ménot and Bard* [2012]. Concentrations of individual GDGT were determined by relating chromatogram peak areas to the concentration of the internal standard C46-GDGT, as proposed by *Huguet et al.* [2006a]. The relative response factor between synthetic (C46-GDGT) and natural GDGTs (GDGT-0) was determined twice a week during running time and was taken into account in the calculation of individual GDGT concentrations, given in μg/g of dry weight sediment [*Huguet et al.*, 2006a]. Selected apolar fractions were analyzed as described above, confirming the efficiency of the automatic separation made by the Gilson system. Analytical procedures at CEREGE (Centre Européen de Recherche et d'Enseignement des Géosciences de l'Environnement) were tested in the two Round Robin experiments for TEX$_{86}$ and BIT analyses, providing favorably comparable results to other laboratories [*Schouten et al.*, 2009, 2013a]. The TEX$_{86}$ or TEX$^{H}_{86}$ ratios were calculated according to *Schouten et al.* [2002] or *Kim et al.* [2010] (equations (2) or (4)).

Similarly to the alkenones, a homogenized standard sediment from the core catcher of MD95-2042 went through chemistry and analysis. The six replicates gave an analytical precision better than ± 0.005 ($\pm 0.4°C$) for TEX$_{86}$ and below 10% for iGDGT concentrations.

3.3. Present and Paleo Tproxy Simulations for the Iberian Margin
3.3.1. Model Description, Grid Choice, and Parameterization
The numerical ocean model used in this study is the Regional Ocean Modeling System (ROMS) [*Shchepetkin and McWilliams*, 2005; *Penven et al.*, 2006]. ROMS is a free-surface, topography-following coordinate model, which solves primitive equations based on Boussinesq and hydrostatic approximations, and uses advection/diffusion schemes for potential temperature and salinity as well as a nonlinear equation of state.

Our numerical configuration for the Iberian Margin is close to the one used in recent studies [*Nolasco et al.*, 2013; *Pires et al.*, 2013, 2014; *Rocha et al.*, 2013]: the domain is limited to 34.5°N–45.5°N and 16.5°W–5.5°W, with a resolution of 1/10° (~9 km) and 30 sigma vertical levels with a stretching factor of $h_s = 6$ and $h_b = 0$ to conserve a good near-surface resolution over the entire domain. The bathymetry is based on ETOPO2 [*National Geophysical Data Center*, 2001], with corrections near the slope and a smoothing filter $r = \text{grad}(h)/h = 0.25$. This resolution implies a time step of 18 min.

All four boundaries of the domain are set open, including the connection to the Mediterranean Sea through Gibraltar Strait, which allows Mediterranean outflow occurrence and the flow of Mediterranean waters over the Gulf of Cadiz and the Iberian Margin. The regional model requires an initial setup, as well as boundary conditions and forcings. These latter are extracted from observational data sets or existing global simulation results according to the considered climate state (present or past) (see section 3.3.2 for the definitions of each simulation and associated forcings).

3.3.2. Present and Paleosimulations: PD-LGM-HS and Associated Forcings
Three different climate mode simulations are conducted using different inputs applied to the same ROMS domain configuration.

3.3.2.1. Present Day (PD) Inputs
The World Ocean Atlas 2005 [*Locarnini et al.*, 2006; *Antonov et al.*, 2006] is used for initial conditions for the temperature and salinity fields and along the domain boundaries providing open boundary conditions. Comprehensive Ocean-Atmosphere Data Set (COADS) monthly mean climatology [*Slutz et al.*, 1985; *da Silva et al.*, 1994] includes the surface forcing fields required for ROMS: sea level pressure, surface air temperature, radiation fluxes (longwave, shortwave, and net heat balance—the latter including latent and sensible heat transfers), water flux into the ocean (evaporation minus precipitation), SST, sea surface salinity (including

the local effect of the discharge of the world's main rivers), wind stress (zonal and meridional components), and specific humidity.

3.3.2.2. Last Glacial Maximum (LGM) and Heinrich Stadial (HS) Inputs

The Institut Pierre-Simon Laplace Coupled Model version 4 (IPSL-CM4) [*Marti et al.*, 2006, 2010] outputs, provided by L. Bopp and V. Mariotti (LSCE, Saclay, France) (Table S2), present all the variables required for ROMS initial setup, boundary conditions, and surface forcings as presented above. IPSL-CM4 outputs are interpolated on the ROMS grid, which is similar to the PD grid, but with sea level decreased by 120 m for realistic glacial coastline position and continental shelf extent.

The mean for the last 50 years (year 500 to year 549) of the IPSL-CM4 steady state simulation known as "LGM" [*Kageyama et al.*, 2009; *Swingedouw et al.*, 2009] or "GLA" [*Mariotti et al.*, 2012] is used to build LGM ROMS inputs.

To produce HS ROMS inputs, we used the mean for the last 50 years (year 350 to year 399) of the IPSL-CM4 "FWF" hosing experiment [*Kageyama et al.*, 2009; *Swingedouw et al.*, 2009; *Mariotti et al.*, 2012]. In this hosing experiment, starting from LGM IPSL-CM4 steady state simulation, the additional freshwater flux of 0.1 Sv (1 sverdrup $= 10^6 \, \mathrm{m^3 \, s^{-1}}$) in the Atlantic Ocean (north of 40°N) and in the Arctic Ocean—which mimics the iceberg melting during a HS—leads to the collapse of the Atlantic Meridional Overturning Circulation (AMOC) in 250 years of simulation (from 15 Sv to 2 Sv). Years 350 to 399 are therefore in an AMOC shutdown "equilibrium," coherent with Heinrich Stadial configurations [*Bond et al.*, 1992; *McManus et al.*, 2004; *Gherardi et al.*, 2005].

### 3.3.3. Tproxy Encoding With Parameterized Production

In this study, the "Tproxy" (modeled temperature proxy) is the modeling tool that considers the chain of processes occurring in the oceanic realm for an organic compound recording oceanic temperatures. The Tproxies are presumed to mimic organic biomarkers which would record the temperature of their environment when produced and which would undergo mixing, advection, and export to the seafloor. Each Tproxy carrier records in situ temperature when produced. To do so, an association of two passive tracers is introduced into the model: the carrier mass (representing the amount of alkenones or GDGTs) and the mass multiplied by the temperature (representing the temperature signal carried by organic proxies). Because both tracers have extensive properties through transport processes, the recorded temperatures are obtained by dividing the latter tracer by the former. The Tproxy carrier undergoes mixing, advection, and has a characteristic time of degradation (exponential decrease) to represent natural remineralization of particulate organic matter. This characteristic time of degradation is set at 3 months for all experiments. A sensitivity test on this residence time, between 1 month and 1 year, gave comparable mean temperature results for Tproxies on the seafloor (±0.5°C). The sinking speed is 5 m/d, equivalent to the sinking rate of small particulate organic carbon in the PISCES biogeochemical model [*Aumont et al.*, 2003; *Aumont and Bopp*, 2006].

The Tproxy tool is thought to represent either alkenone-based or GDGT-based organic proxies, and the many possible configurations allow us to test the effect of season and depth of production for each Tproxy carrier on its final temperature record on the seafloor. A combination of two depths (surface and 0–200 m) and three seasons (annual, summer, and winter) is tested with the Tproxy tool, to cover the range of possible production conditions (see section 2). We run six parameterized functions of production for each climate mode (Table S2). First, a constant Tproxy production on the whole surface of the oceanic domain is considered, with three seasons tested: annual surface production (ASP), summer surface production, and winter surface production. Second, a constant Tproxy production on the 0–200 m depth interval of the marine field is tested, again with three seasons considered: annual 0–200 m depth production, summer 0–200 m depth production, and winter 0–200 m depth production (Table S2). The constant surface production rate is set at $10^{-9} \, \mathrm{mg/m^2/s}$, which leads to proxy carrier mean concentrations similar to $10^{-5} \, \mathrm{mg/m^3}$ in Tproxy ASP steady state simulation.

In order to be directly comparable to sedimentary organic proxy results, Tproxy results are shown as the annually averaged temperature of the Tproxy carrier flux at the water-sediment seafloor interface. We do not include sediment reworking, transport, or diagenetic processes in the Tproxy tool.

3.3.4. Conducted Simulations

Modern climatologies (e.g., World Ocean Atlas 2005, 1° × 1° resolution) or general circulation models for past climate states (e.g., IPSL-CM4, 2° × 1.5° resolution) (Figure 1c) do not allow to represent the specific fine oceanographic features off Portugal in terms of currents and temperatures with adequate resolution (summer upwelling along the coast, upwelling filaments, meanders, and offshore currents). The regional ocean model
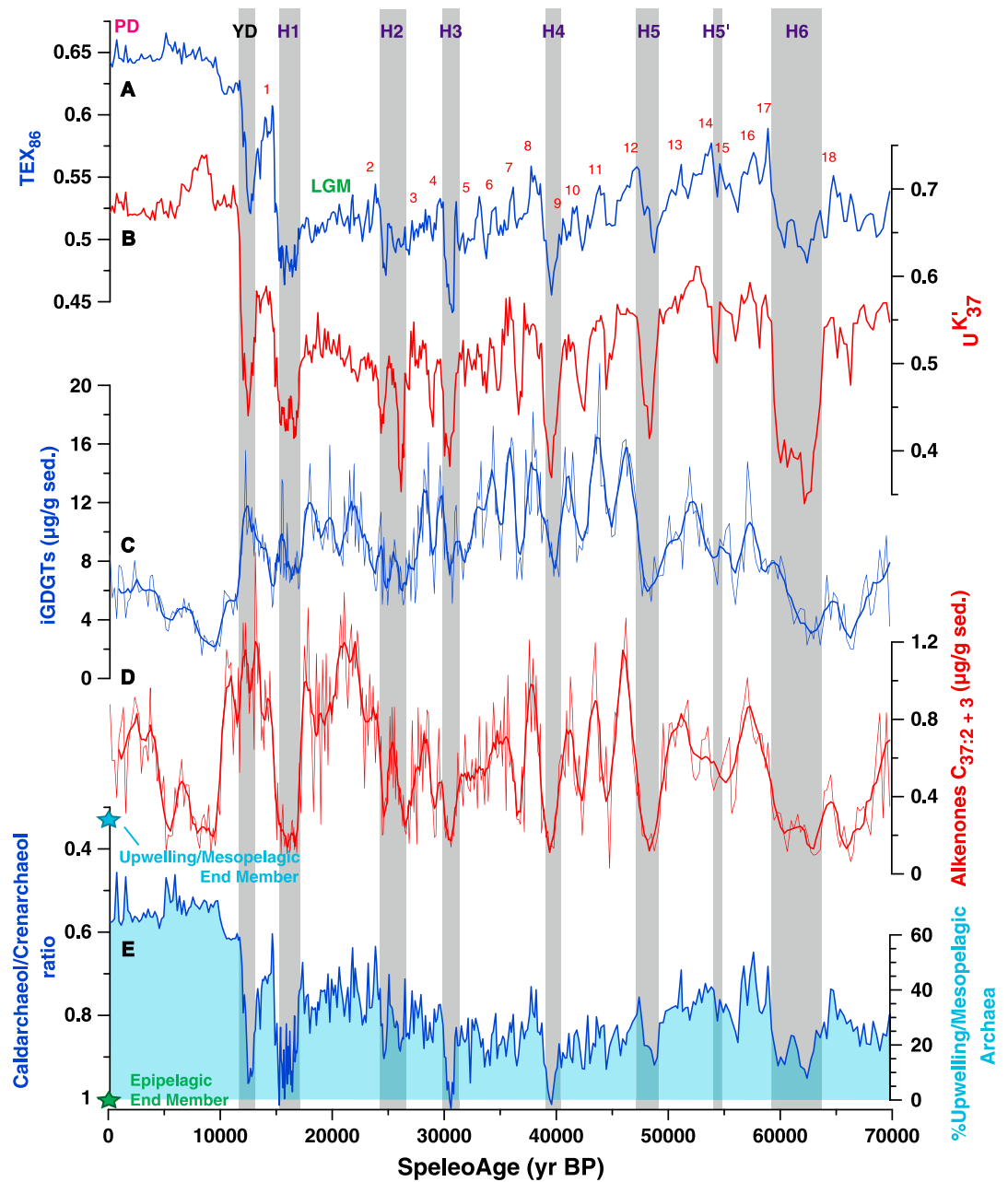
Figure 2. Biomarker results for core MD95-2042. (a) TEX_{86} and (b) $U^{K'}_{37}$ indices and biomarker concentrations (thick line = least squared 2–3 smoothing on 11 points): (c) isoprenoid GDGTs and (d) alkenones $C_{37:2} + C_{37:3}$. (e) Caldarchaeol/Crenarchaeol ratio (on the left-hand side axis) or contribution of upwelling/mesopelagic Archaea to TEX_{86} signal (on the right-hand axis) calculated after using a bipolar mix model between two Caldarchaeol/Crenarchaeol ratio end-members: light blue and green stars represent "pure" upwelling/mesopelagic Archaea and Epipelagic Archaea end-members, respectively, as proposed by *Turich et al.* [2007]. Grey bars refer to cold events: YD = Younger Dryas and H1 = Heinrich Stadial 1. Red numbers refer to warm Dansgaard/Oeschger events, also called Greenland Interstadial (GIS) events. PD = Present Day and LGM = Last Glacial Maximum.

ROMS has been chosen for its capacity to represent such fine oceanographic features at meander scale (1/10° resolution) (Figure 1b) with monthly and interannual variability. This is particularly required when considering the intermediate position of the core, which was taken at a location between inshore and offshore with relation to the coastal upwelling.

Table S2 presents a summary of Tproxy experimental design and conducted simulations. Each simulation is run for 125 years and provides monthly mean outputs. For all three climate modes (PD, LGM, and HS; see section 3.3.2),
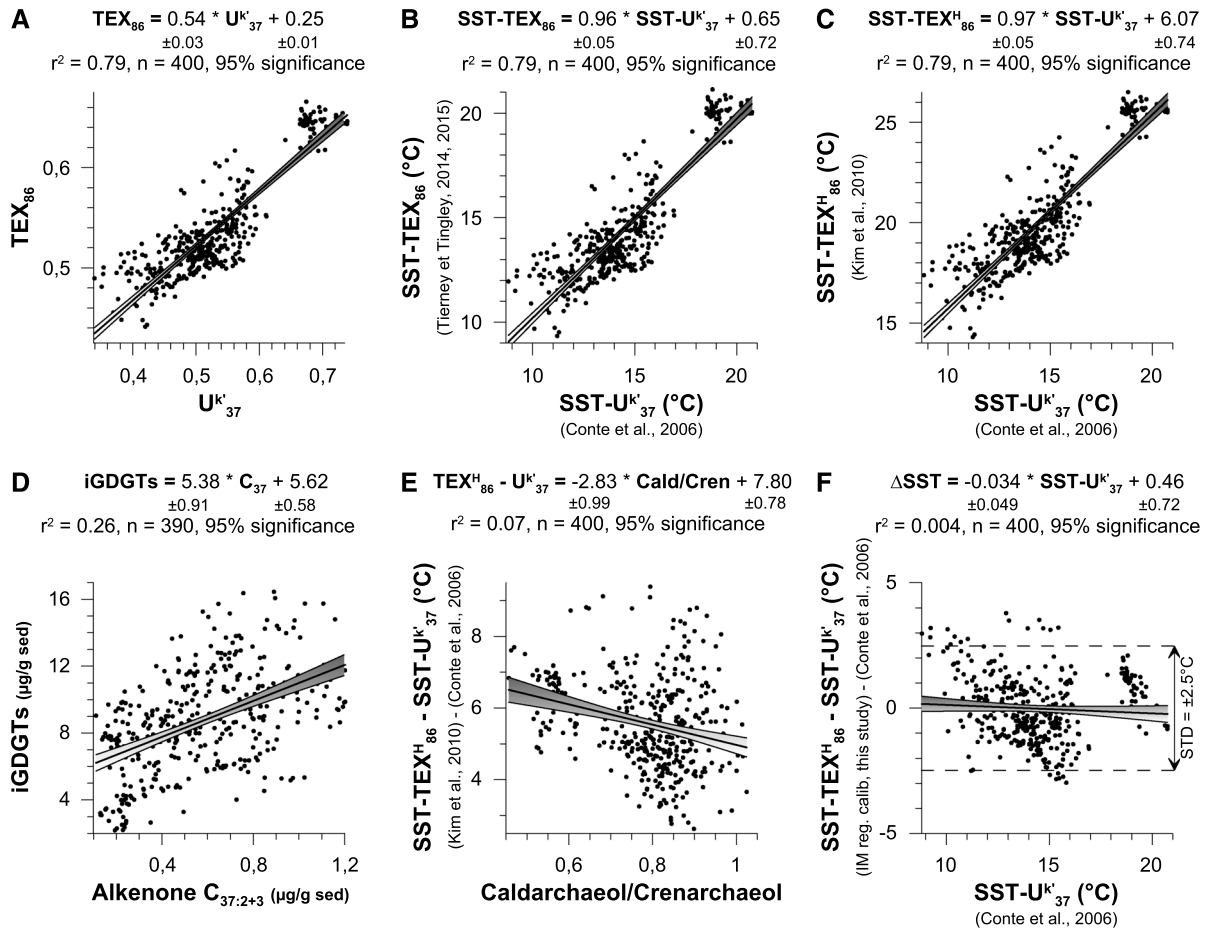
Figure 3. Correlations between different biomarker parameters in core MD95-2042 during the last 70 kyr. (a) TEX_{86} and $U^{K'}_{37}$, (b) SST-TEX_{86} [*Tierney and Tingley*, 2014, 2015] and SST-$U^{K'}_{37}$ [*Conte et al.*, 2006], (c) SST-TEX^H_{86} [*Kim et al.*, 2010] and SST-$U^{K'}_{37}$ [*Conte et al.*, 2006], (d) iGDGT concentration and alkenone $C_{37:2+3}$ concentration (µg/g sediment), (e) SST-TEX^H_{86} − SST-$U^{K'}_{37}$ [*Kim et al.*, 2010; *Conte et al.*, 2006] and Caldarchaeol/Crenarchaeol ratio, and (f) SST-TEX^H_{86} − SST-$U^{K'}_{37}$ (this study's regional calibration) [*Conte et al.*, 2006] and SST-$U^{K'}_{37}$ [*Conte et al.*, 2006].

the total kinetic energy of the Iberian Margin oceanic volume stabilizes in 3 years of simulation time, the circulation reaching a steady state, with interannual variability of <5%. The six Tproxy experiments are conducted on the three previously described climate modes for the final 15 years (years 111 to 125). Both Tproxy passive tracers stabilize after 3 years of simulation. Therefore, the following results and discussion will be based on the monthly mean of the final 10 years of simulation (years 116 to 125).

4. Results

### 4.1. TEX_{86} and $U^{K'}_{37}$ Indices and Associated Biomarker Concentrations

Core MD95-2042 biomarker results are presented in Figure 2 for both indices and associated compound concentrations. For the last 70 kyr, TEX_{86} ranges between 0.44 and 0.67 (Figure 2a), while $U^{K'}_{37}$ varies between 0.34 and 0.74 (Figure 2b). The average value is higher during the Holocene (interglacial period) ($n = 56$, 0.64 ± 0.01 for TEX_{86}, and 0.69 ± 0.02 for $U^{K'}_{37}$) than during the last glacial (except Heinrich Stadials) ($n = 239$, 0.52 ± 0.02 for TEX_{86}, and 0.52 ± 0.04 for $U^{K'}_{37}$), which in turn is higher than during Heinrich Stadials ($n = 68$, 0.49 ± 0.02 for TEX_{86}, and 0.42 ± 0.03 for $U^{K'}_{37}$). TEX_{86} and $U^{K'}_{37}$ show in-phase abrupt climate variability for the last glacial and termination 1, which is characteristic of the North Atlantic signal: synchronous cold events (Dansgaard/Oeschger Stadials) and warm events (Dansgaard/Oeschger Interstadials, red numbers in Figure 2a), as well as intense North Atlantic cold events (Heinrich Stadials, areas shaded grey and purple numbers in Figure 2), are observed, as previously reported for

Table 1. Published TEX_{86} and $U_{37}^{K'}$ Temperature Calibrations[a]

Reference	Index	Temperatures Used for Calibration	Type	Statistics	Equation	Temperature Range (°C)
Schouten et al. **[2002] EPSL**	TEX_{86}	Annual mean SST	Global, core top	Linear regression	$SST = (TEX_{86} - 0.28)/0.015$ $(n = 44, r^2 = 0.92, STD = 2.0°C)$	[0; 30]
Wuchter et al. [2004] Paleoceanography	TEX_{86}	In situ temperature	Culture (mesocosm) (10–30°C)	Linear regression	$T = (TEX_{86} - 0.1)/0.015$ $(n = 15, r^2 = 0.79)$	[10; 25]
Wuchter et al. [2005] Paleoceanography	TEX_{86}	Annual mean SST	Particulate organic matter in marine water column (<100 m) + core tops	Linear regression	$SST = (TEX_{86} - 0.29)/0.015$ $(n = 61, r^2 = 0.92)$	[5; 30]
Schouten et al. [2007] OG	TEX_{86}	In situ temperature	Culture (mesocosm) (10–40°C)	Linear regression	$T = (TEX_{86} - 0.064)/0.017$ $(n = 21, r^2 = 0.86)$	[10; 30]
Kim et al. **[2008] GCA**	TEX_{86}	Annual mean SST	Global, core top	Linear regression	$SST = 56.2 \times TEX_{86} - 10.8$ $(n = 223, r^2 = 0.935, STD = 1.7°C)$	[0; 30]
Liu et al. [2009] Science	TEX_{86}	Annual mean SST	Global, core top	Linear regression	$SST = -16.3 \times (1/TEX_{86}) + 50.5$ $(n = 287, r^2 = 0.817)$	[5; >30]
Kim et al. **[2010] GCA**	TEX_{86}^L	Annual mean SST	Global, core top	Linear regression	$SST = 67.5 \times TEX_{86}^L + 46.9$ $(n = 396, r^2 = 0.86, STD = 4.0°C)$	<15
	TEX_{86}^H	Annual mean SST	Global, core top	Linear regression	$SST = 68.4 \times TEX_{86}^H + 38.6$ $(n = 255, r^2 = 0.87, STD = 2.5°C)$	[15; 28]
Kim et al. [2010] GCA (data from *Wuchter et al.* [2004] and *Schouten et al.* [2007])	TEX_{86}^H	In situ temperature	Culture (mesocosm)	Linear regression	$T = 52.0 \times TEX_{86}^H + 42.0$ $(n = 21, r^2 = 0.84)$	[10; 30]
Kim et al. **[2012] EPSL**	TEX_{86}^H	0–200 m annual mean temperature (WOA 2009)	Global, core top	Linear regression	$0{-}200\ m\ T = 54.7 \times TEX_{86}^H + 30.7$ $(n = 255, r^2 = 0.84)$	[5; 25]
Tierney and Tingley **[2014] GCA**	TEX_{86}	Annual mean SST (WOA 2009)	Spatially evolving, core top	Bayesian	x	all
Prahl and Wakeham [1987] Nature	U_{37}^K	In situ temperature	Culture *E. huxleyi*	Linear regression	$T = (U_{37}^K + 0.11)/0.04$	[8; 25]
Prahl et al. **[1988] GCA**	$U_{37}^{K'}$ $U_{37}^{K'}$	In situ temperature	Culture *E. huxleyi*	Linear regression	$T = (U_{37}^{K'} + 0.043)/0.033$ $T = (U_{37}^{K'} + 0.039)/0.034$ $(r^2 = 0.994)$	[8; 25]
Rosell-Melé et al. [1995] GCA	U_{37}^K	Annual mean SST	Northeastern Atlantic, core top	Linear regression	$SST = (U_{37}^K) - 0.162/0.029$ $(n = 109, r^2 = 0.958)$	[0; 28]
Müller et al. **[1998] GCA**	$U_{37}^{K'}$	Annual mean SST	Global, core top	Linear regression	$SST = (U_{37}^{K'} + 0.044)/0.033$ $(n = 370, r^2 = 0.958, STD = 1.5°C)$	[0; 29]
Conte et al. [2006] G3	$U_{37}^{K'}$	Annual mean SST	Global, core top	Linear regression	$SST = 29.876 \times U_{37}^{K'} - 1.334$ $(n = 592, r^2 = 0.97, STD = 1.1°C)$	[0; 30]

[a]Bold equations and references are those used and plotted in Figure 4.
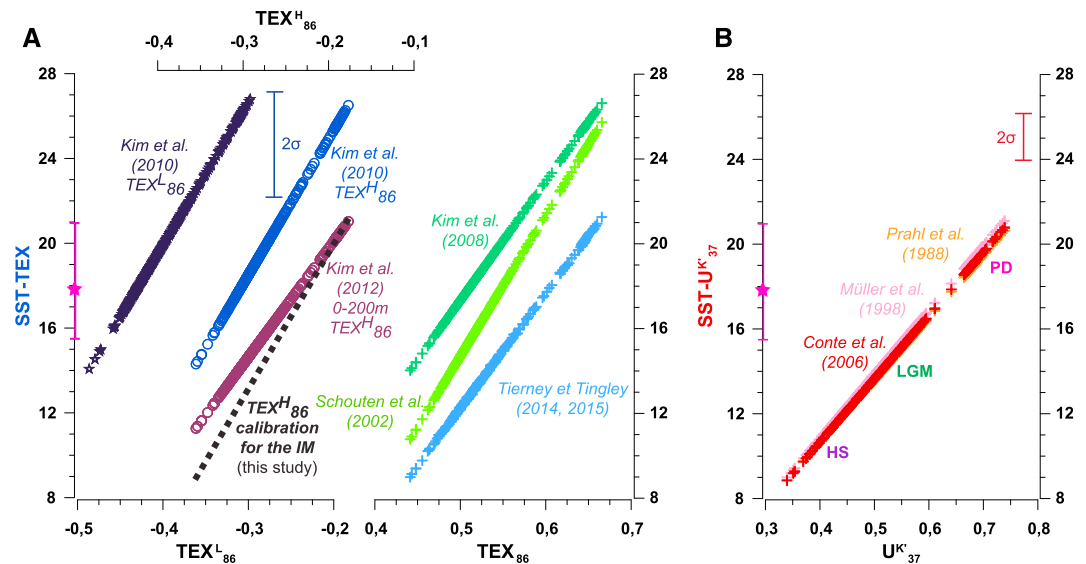
Figure 4. SST reconstructions for core MD95-2042 based on different published linear calibrations. (a) SST-TEX$_{86}$ versus TEX index: dark purple stars for TEX$_{86}^L$ annual mean SST calibration [*Kim et al.*, 2010]; dark blue circles for TEX$_{86}^H$ annual mean SST calibration [*Kim et al.*, 2010] and associated dark blue 2σ error bar, purple circles for TEX$_{86}^H$ 0–200 m annual mean calibration [*Kim et al.*, 2012], and black dotted line for TEX$_{86}^H$ annual mean SST calibration for the Iberian Margin (this study); and green crosses [*Kim et al.*, 2008], light green crosses [*Schouten et al.*, 2002], and light blue crosses [*Tierney and Tingley*, 2014, 2015] for TEX$_{86}$ annual mean SST calibrations. (b) SST-U$_{37}^{K'}$ versus U$_{37}^{K'}$: orange crosses for U$_{37}^{K'}$ culture calibration [*Prahl et al.*, 1988] and pink crosses [*Müller et al.*, 1998] and red crosses with associated red 2σ error bar [*Conte et al.*, 2006] for sedimentary U$_{37}^{K'}$ annual mean SST calibration. The pink stars represent the present-day annual mean SST at the core site, while the associated pink bars show the maximum and minimum monthly SST at the core site. PD = Present Day; LGM = Last Glacial Maximum; and HS = Heinrich Stadial.

the Iberian Margin [e.g., *Pailler and Bard*, 2002; *Martrat et al.*, 2007]. Raw TEX$_{86}$ and U$_{37}^{K'}$ signals display a significant positive correlation for the last 70 kyr ($R^2 = 0.79$, $n = 400$) (Figure 3a).

The BIT values are low, ranging from 0.01 to 0.06 with average values identical for the Holocene (0.03 ± 0.006, $n = 56$) and the last glacial (0.02 ± 0.008, $n = 307$) (not shown).

Concentrations of the marine isoprenoid GDGTs vary between 1.6 and 21.5 µg/g dry sediment (Figure 2c), while those of C$_{37}$ alkenones range between 0.1 and 1.7 µg/g dry sediment (Figure 2d). Smoothed concentrations (least squares 2–3 procedure on 11 points [*Savitzky and Golay*, 1964]) of iGDGTs and C$_{37}$ alkenones exhibit a positive correlation ($R^2 = 0.26$, $n = 390$) (Figure 3d). Both concentrations are higher during the glacial period excluding Heinrich Stadials than during the Holocene. Abrupt climate variability of the last glacial is also marked in both smoothed concentrations, with higher values during Dansgaard/Oeschger Interstadials and low concentrations during Heinrich Stadials (Figures 2c and 2d).

The Caldarchaeol/Crenarchaeol ratio (GDGT-0/GDGT-4) was proposed by *Turich et al.* [2007] to evaluate the variation of archaeal group contributions to the GDGT-based SST reconstructions. A binary mixing model is applied to the Caldarchaeol/Crenarchaeol ratio using two end-member values for upwelling/mesopelagic origin or for epipelagic origin (Figure 2e). The Caldarchaeol/Crenarchaeol ratio shows high variability for the last 70 kyr, with values between 0.46 and 1.02 (i.e., 0 to 81% of upwelling/mesopelagic Archaea) (Figure 2e). A smaller ratio (higher upwelling/mesopelagic contribution) is observed for the Holocene ($n = 56$, 67 ± 5% upwelling/mesopelagic) than for the last glacial ($n = 239$, 28 ± 9% upwelling/mesopelagic) or for Heinrich Stadials ($n = 68$, 14 ± 8% upwelling/mesopelagic) (Figure 2e).

4.2. SST-TEX$_{86}$ and SST-U$_{37}^{K'}$ Reconstructions

The different versions of the TEX$_{86}$ index (TEX$_{86}$, TEX$_{86}^L$, and TEX$_{86}^H$) and associated calibrations (Table 1) give different temperature ranges for the last 70 kyr of core MD95-2042 based on the same iGDGT distributions (Figure 4a). The temperature relationship based on mesocosm experiments [*Kim et al.*, 2010; after *Wuchter et al.*, 2004; *Schouten et al.*, 2007] gives higher values (between 23.5°C and 32.8°C) than global core top sediment
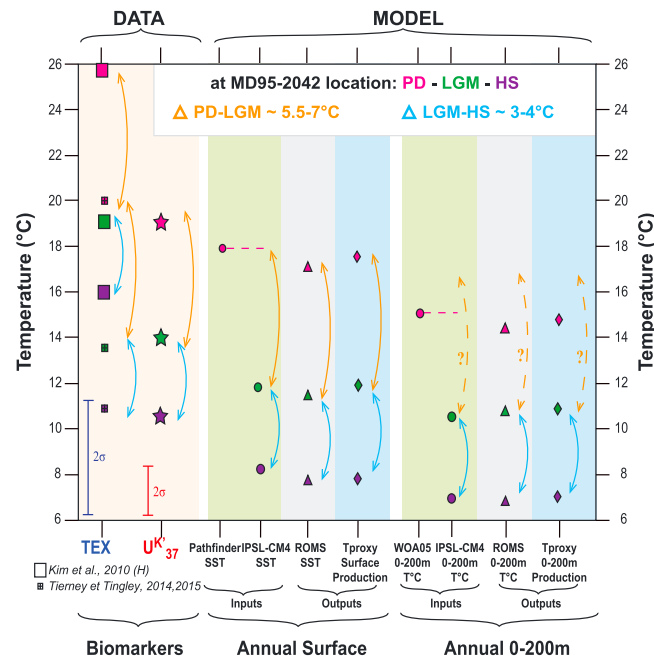
Figure 5. A data-model comparison of annual mean temperatures at MD95-2042 core site for three climate modes. Pink symbols reflect Present Day conditions, green symbols indicate the Last Glacial Maximum, and purple symbols refer to Heinrich Stadials. (left) The mean reconstructed SSTs via biomarkers for each climate mode (light orange): TEX_{86} results with big squares [*Kim et al.*, 2010] and small crossed squares [*Tierney and Tingley*, 2014, 2015] show the range of reconstructed SST with the different calibrations; stars represent mean $U_{37}^{K'}$ results [*Conte et al.*, 2006]. The error bars (2σ) associated with TEX_{86} and $U_{37}^{K'}$ calibrations are also reported. Annual mean temperature inputs (green panels) and outputs (grey and blue panels) for ROMS simulations are presented for surface and 0–200 m depth interval. Small circles show ROMS inputs (PD observation: Pathfinder/World Ocean Atlas 2005; LGM and HS: IPSL-CM4 [*Mariotti et al.*, 2012]), small triangles represent ROMS temperature outputs (mean year 116 to year 125), and small diamonds show annual (surface or subsurface) production Tproxy results (mean years 116–125). Orange arrows show the temperature difference between LGM and PD. Light blue arrows show the temperature difference between HS and LGM. Question marks associated with 0–200 m orange arrows show that there is no match with the biomarker data. However, TEX_{86} and $U_{37}^{K'}$ deltas between climate modes correspond to modeled annual surface deltas, which supports the suggestion that biomarkers do record annual surface temperatures.

linear calibrations based on annual mean SSTs (10.8°C–25.7°C [*Schouten et al.*, 2002] or 14.0°C–26.6°C [*Kim et al.*, 2008] for TEX_{86} index, 14.1°C–26.8°C for TEX_{86}^L [*Kim et al.*, 2010], and 14.3°C–26.5°C for TEX_{86}^H [*Kim et al.*, 2010]) (Figure 4a). TEX_{86}^H calibration based on mean annual 0–200 m temperature [*Kim et al.*, 2012] shows smaller values (between 11.3°C and 21.0°C) (Figure 4a). The different global linear calibrations tested for TEX_{86}-SST reconstructions (Table 1 and Figure 4) give a wide range of results for MD95-2042 core top samples. Using annual mean SST-based calibrations, modern TEX_{86} temperature reconstructions (late Holocene, $n = 35$, STD = ±0.4°C) (± standard calibration error) are between 24.5°C ± 2.0°C and 25.6°C ± 1.7°C for TEX_{86} (*Schouten et al.* [2002] and *Kim et al.* [2008], respectively) and 25.7°C ± 2.5°C and 26.1°C ± 4.0°C for TEX_{86}^H and TEX_{86}^L, respectively [*Kim et al.*, 2010] (Figure 4). The mesocosm calibration gives even warmer results of around 32.2°C [*Kim et al.*, 2010; after *Wuchter et al.*, 2004; *Schouten et al.*, 2007], while the global annual mean 0–200 m temperature-based calibration gives 20.4°C for the modern samples ($n = 35$) [*Kim et al.*, 2012] (Figure 4). All these results are unrealistically warm, even when calibration errors are taken into account, in comparison to present-day temperature observations at MD95-2042 location (satellite annual mean SST of 18.0°C and annual mean 0–200 m temperature of 15.3°C) [*Casey and Cornillon*, 1999; *Armstrong and Vazquez-Cuervo*, 2001; *Locarnini et al.*, 2006; *Casey et al.*, 2010] (Figure 5). All

TEX linear calibrations (referring to all TEX indices: TEX_{86}, TEX_{86}^L, and TEX_{86}^H) thus lead to significantly higher temperature results than with $U_{37}^{K'}$ SST (Figure 4). However, using the recently developed Bayesian spatially varying calibration with its updated database [*Tierney and Tingley*, 2014, 2015] (with BAYSPAR inputs: prior STD of 5°C, minimum number of core top data = 1, maximum distance = 500 km; number of samples for Monte Carlo draw = 5000), the temperature range covered by MD95-2042 TEX_{86} data for the last 70 kyr is between 9.3°C and 21.1°C (Figure 4a), which is closer to $U_{37}^{K'}$ SST reconstructions (Figure 4b). Modern TEX_{86} temperatures are around 20.2°C ± 4.4°C (mean calculated error on the calibration holding 90% of the Bayesian signal variance), which is comparable to present-day annual mean SST at the core site (18.0°C)—within error.

In the following sections, we present and discuss our TEX-based temperature results with the most recent global linear calibration for annual mean SST reconstructions (TEX_{86}^H) [*Kim et al.*, 2010] (Figure 4a, dark blue circles), which is of late the most commonly used calibration for temperature reconstructions based on isoprenoid GDGTs [*Huguet et al.*, 2011; *McClymont et al.*, 2012; *Nakanishi et al.*, 2012b; *Seki et al.*,
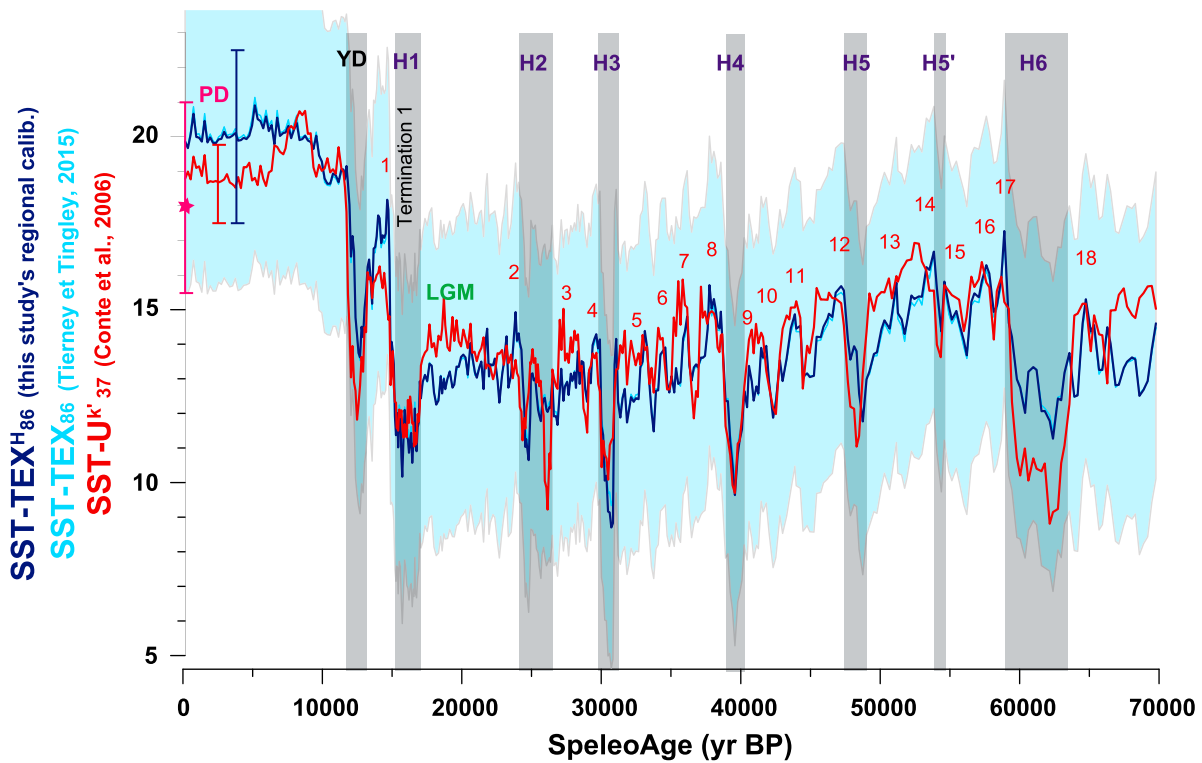
Figure 6. Annual mean SST reconstructions based on $U_{37}^{K'}$ [*Conte et al.*, 2006] (red) and TEX_{86} [*Tierney and Tingley*, 2014, 2015] (light blue) or TEX_{86}^{H} (this study's Iberian Margin calibration) (dark blue) in core MD95-2042 for the last 70 ka B.P. The light blue shaded area shows the Bayesian error (confidence interval of 95%) for TEX_{86} temperature reconstructions with the calibration by *Tierney and Tingley* [2014, 2015]. The pink star represents the present-day annual mean SST at the core site, while the associated pink bar shows the maximum and minimum monthly SST at the core site. Grey bars refer to cold events: YD = Younger Dryas and H1 = Heinrich Stadial 1. Red numbers refer to warm Dansgaard/Oeschger events, also called Greenland Interstadial (GI) events. PD = Present Day and LGM = Last Glacial Maximum.

2012; *Yamamoto et al.*, 2012; *Grauel et al.*, 2013; *Lopes dos Santos et al.*, 2013; *Nieto-Moreno et al.*, 2013; *Shaari et al.*, 2013; *Smith et al.*, 2013; *Zhang et al.*, 2013; *Basse et al.*, 2014; *Hernández-Sánchez et al.*, 2014; *O'Brien et al.*, 2014; *Zhang et al.*, 2014; *Ho and Laepple*, 2015], and compare these results with the Bayesian calibration-derived temperatures which take regional effects into account [*Tierney and Tingley*, 2014, 2015] (Figure 6, light blue).

Concerning $U_{37}^{K'}$, both calibrations based either on cultured organisms at different temperatures [*Prahl et al.*, 1988] or on worldwide core top data compared to annual mean SST [*Müller et al.*, 1998; *Conte et al.*, 2006] give comparable temperature results for core MD95-2042 for the last 70 kyr, of between 8.8°C and 20.7°C (Figure 4b), as well as for modern samples (core top and late Holocene: 18.9 ± 0.3°C, *n* = 35). For the following discussion, the most recent and complete (large data set) calibration is used [*Conte et al.*, 2006] for the reconstruction of past annual mean SSTs for core MD95-2042 (Figure 6).

4.3. Tproxy Results

Tproxies record modeled in situ temperature when their mass is produced, and they undergo advection through surface and subsurface currents prior to export to the seafloor. The validity of simulated physics, especially in terms of temperature and currents, is therefore a crucial point which needs to be evaluated prior to any consideration of Tproxy results. Physical parameters of present and past simulations are assessed in Text S7 (supporting information).

For all three climate modes, oceanic temperature characteristics (seasonality, annual mean, and spatial distribution) are preserved and transmitted between ROMS inputs (modern climatologies or IPSL-CM4), ROMS outputs (simulated temperatures), and the tested Tproxies, as being particularly well observed for core MD95-2042 (Table 2 and Figure 5 for annual means).

Table 2. ROMS Temperature Inputs and Outputs and Tproxy Results at MD95-2042 Site

Climate Mode	Season	Depth	Model Input, T (°C)	ROMS Output, T (°C)	Tproxy (°C)
PD			*Pathfinder*		
	Annual	Surface production	18.0	17.1	17.4
	Maximum/summer		21.0	20.4	20.8
	Minimum/winter		15.5	14.2	14.9
			WOA 05		
	Annual	0–200 m production	15.3	14.3	14.7
	Maximum/summer		16.0	15.1	15.3
	Minimum/winter		14.7	13.6	14.2
LGM			*IPSL-CM4 GLA*		
	Annual	Surface production	12	11.6	11.8
	Maximum/summer		14.2	12.9	13.3
	Minimum/winter		10.2	10.3	10.4
	Annual	0–200 m production	10.5	10.6	10.8
	Maximum/summer		10.9	10.8	11.0
	Minimum/winter		10.1	10.3	10.4
HS			*IPSL-CM4 FWF*		
	Annual	Surface production	8.2	7.5	7.8
	Maximum/summer		10.3	9.0	9.5
	Minimum/winter		6.4	6.1	6.5
	Annual	0–200 m production	6.9	6.8	7.0
	Maximum/summer		7.2	7.1	7.2
	Minimum/winter		6.6	6.6	6.8

Tproxy with annual surface production, for the Present Day, duplicates the SST annual means on the whole Iberian Margin. At the core site, it gives 17.4°C, comparable to the satellite annual mean SST value of 18°C (Table 2 and Figure 5).

The difference between summer surface production and winter surface production Tproxies for PD is comparable to the SST seasonality for the Iberian domain, except for along the coast, where values of SST seasonality lower than the climatology are observed (~2°C) due to the cold summer waters of the intense upwelling simulated by ROMS-PD. This Tproxy difference is ~6°C at MD95-2042 location, similar to Pathfinder climatology and to ROMS modeled SST seasonal amplitudes (Table 2).

Tproxy with annual 0–200 m production shows values comparable to temperatures of the 0–200 m depth interval at MD95-2042 core site, of around 15°C for ROMS inputs and outputs for PD simulation (Table 2 and Figure 5).

The seasonal amplitude for the subsurface is captured by Tproxies with 0–200 m depth production (summer 0–200 m production minus winter 0–200 m production), showing much lower values than at the surface for PD: between 0.5 and 2°C for the Iberian Margin domain and 1°C at the core site (Table 2).

For LGM and HS states, similar comparison between ROMS inputs, outputs, and Tproxies can be conducted in the same way as previously described for PD. Simulated annual mean temperatures are transmitted to the Tproxies with annual production, for both surface and 0–200 m depth productions, as observed at MD95-2042 location (Table 2 and Figure 5). Similar seasonal amplitudes between ROMS temperature outputs and both Tproxies with surface and 0–200 m production are observed (~3°C and ~0.5°C for surface and 0–200 m, respectively) (Table 2).

Considering temperature amplitudes between climate modes, LGM annual surface production Tproxy shows temperatures colder than for PD: between −2°C and −7°C for the Iberian domain, with variability at a scale of 100 km forming meanders (Figure 7b1). At the MD95-2042 location, this difference is equal to −5.5°C (Figure 5), which is only found southwest or north of the Iberian Peninsula (see Figure 7b1, black line). Heinrich minus Glacial (HS-LGM) differences for annual surface production Tproxy are also subject to local variability on the studied area, with values between −3°C and −5°C, and equal to −4°C at MD95-2042 core site (Figures 7b2 and 5). Therefore, even at the regional scale of the Iberian Margin, large differences in temperature amplitudes between climate modes can be recorded. A combination of climate mode
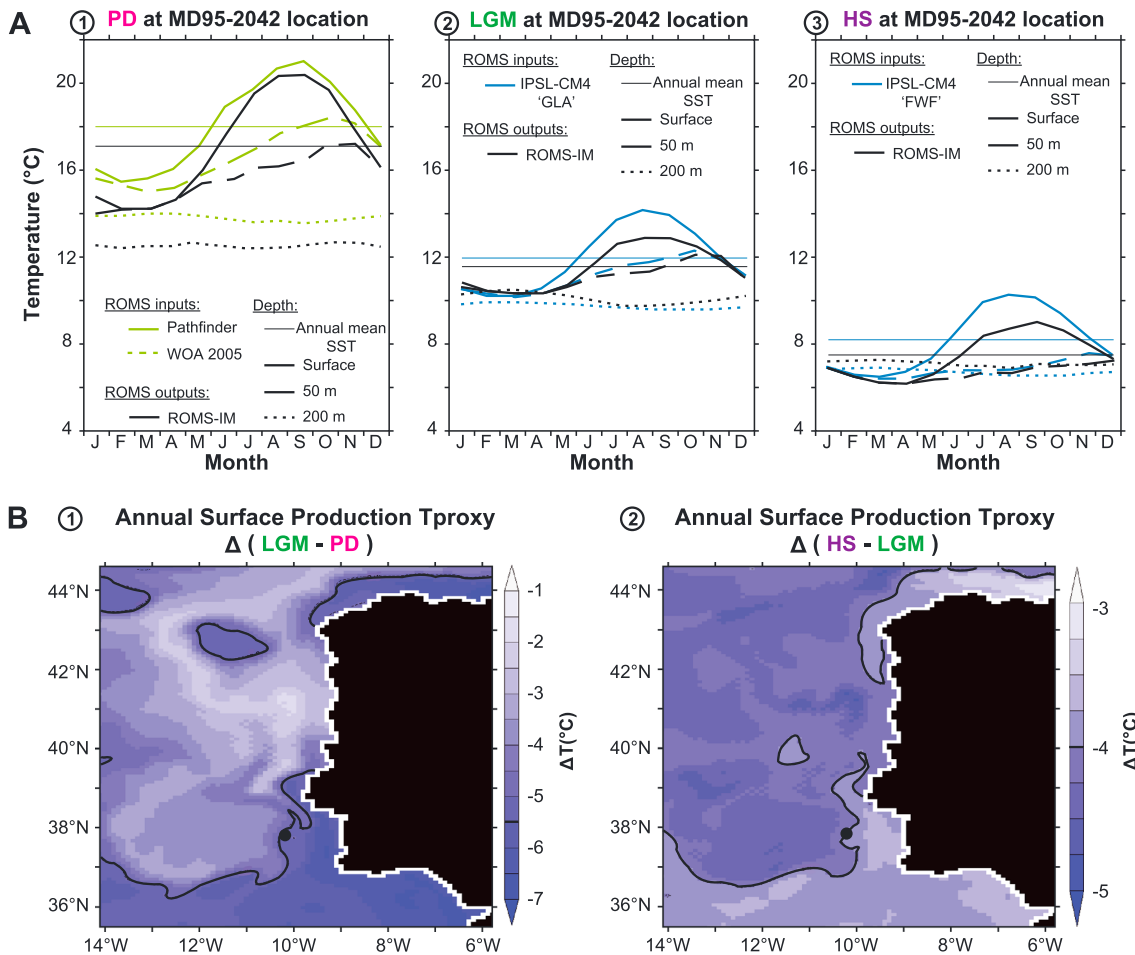
Figure 7. (a) Temperature comparison between forcings (modern climatology IPSL-CM4) and ROMS outputs (mean of the last 10 years of simulation, year 116 to year 125) at MD95-2042 core site, for three climate modes: PD = Present Day (1), LGM = Last Glacial Maximum (2), and HS = Heinrich Stadial (3). (b) Climate mode effect on Tproxy results: LGM-PD (1) and HS-LGM (2) differences for annual surface production Tproxy (mean year 116 to year 125). The black line represents the temperature difference between climate modes recorded at the core site (Δ(LGM-PD) = −5.5°C and Δ(HS-LGM) = −4°C).

temperature differences (e.g., for annual surface production: [Δ(LGM-PD), Δ(HS-LGM)]) is then specific of a location in the Iberian domain.

5. Discussion

5.1. Alkenone Thermometry: Reliable Annual Mean SST?

SST-$U_{37}^{K'}$ results given by the three calibrations based on culture experiments (in situ temperature) [*Prahl et al.*, 1988] and global core top measurements (annual mean SST) [*Müller et al.*, 1998; *Conte et al.*, 2006] are almost identical (Figure 4b). MD95-2042 modern samples (core top + late Holocene samples, to 6 ka B.P.) give a mean SST-$U_{37}^{K'}$ result of 18.9°C (n = 35, STD = 0.3°C) (Figure 6), which is consistent with present-day satellite data at the core site (18.0°C), considering the calibration errors (±1.1°C) [*Conte et al.*, 2006].

Alkenone-based temperature reconstructions in core MD95-2042 are consistent with nearby core MD01-2444 [*Martrat et al.*, 2007] for the present interglacial and the last glacial, with the exception of some Heinrich Stadials (H2, H3, and H6) which appear colder (~ −2°C) in our record (Figure 6). Similar comparisons with published data in the same core MD95-2042 [*Pailler and Bard*, 2002] have already been discussed in Text S6. Previous studies in this area show comparable results with ours and have assumed that the $U_{37}^{K'}$ temperature records represent annual mean SST for present and past glacial-interglacial cycles [*Bard et al.*, 2000; *Bard*, 2001; *Pailler and Bard*, 2002; *Martrat et al.*, 2007; *Rodrigues et al.*, 2011].

We examine the effects of the regional depth and season of alkenone exported production with Tproxy modeling. From direct comparison between average values of MD95-2042 $U_{37}^{K'}$ temperature for each climate mode and different Tproxy results (Figure 5 and Table 2), we can see that PD $U_{37}^{K'}$ data are 18.9°C, similar to the Tproxy with annual surface production of 17.4°C (Figure 5) when calibration (±1.1°C) and Tproxy sensitivity errors (±0.5°C) are taken into account. However, mean PD $U_{37}^{K'}$ temperatures do not match other Tproxies with different season or depth of production: summer and winter surface production Tproxies give values of 20.9°C and 14.9°C, respectively, which are too warm and too cold for possible match; 0–200 m production Tproxies show temperatures between 14.3°C and 15.3°C, which are too cold compared to PD $U_{37}^{K'}$ temperature (18.9°C) (Figure 5). These results support the idea that $U_{37}^{K'}$ reflects annual mean SST with an alkenone production at the surface throughout the year for modern conditions.

For LGM and HS conditions, $U_{37}^{K'}$ temperature reconstructions (14°C and 10°C, respectively) are much warmer than Tproxies with 0–200 m depth production (around 11°C and 7°C for LGM and HS, respectively) (Figure 5). Therefore, $U_{37}^{K'}$ signals do not record a subsurface signal. This thus suggests an unchanged surface production of alkenones for the last 70 kyr (and the corresponding three climate modes). Furthermore, LGM and HS $U_{37}^{K'}$ SST reconstructions are closer to the Tproxy with summer surface production (13.3°C and 9.5°C, respectively) than to any other Tproxy parameterization, which all present colder temperature results (Figure 5 and Table 2). This tendency toward SSTs warmer than the annual mean during the glacial period could be due either to wrongly modeled temperatures (ROMS SST colder than IPSL-CM4 at MD95-2042 position, especially during summer (to −1.5°C) (Figures 7a2 and 7a3)) or to the inaccuracy of the calibration for glacial time, or again, to a seasonal shift of haptophyte productivities toward the warmer season. It is difficult to ascertain which hypothesis is the correct one.

Therefore, the $U_{37}^{K'}$-based temperature signal in core MD95-2042 is interpreted to record present and past annual mean surface temperature (SST), with no apparent change in depth of production, except for a potential shift toward summer production that may occur for glacial times.

5.2. TEX$_{86}$ Thermometry: A Reliable Tool for Absolute Temperature Reconstructions Off Portugal?

The different global linear calibrations tested for TEX$_{86}$ temperature reconstructions give unrealistically warm results for MD95-2042 modern samples compared to present-day temperature observations. Could a shift of season and/or depth of Thaumarchaeota production explain such warm TEX$_{86}^{H}$ temperatures? To clarify the following discussion, we will only use the latest global annual mean SST-based calibration proposed by *Kim et al.* [2010] for TEX$_{86}^{H}$, yet the same reasoning holds true for other global calibration equations (Figure 4a). The mean PD TEX$_{86}^{H}$ temperature estimate (25.7°C) is almost 8°C warmer than the annual mean SST. As modern deeper temperatures are lower than modern SST (Figure 7a1), no shift in the depth of production can be invoked. Modern monthly SSTs in this location display a maximum value of 21.0°C in September [*Casey and Cornillon*, 1999; *Armstrong and Vazquez-Cuervo*, 2001] (Figure 7a1). Even considering the range of calibration error (±2.5°C for TEX$_{86}^{H}$), modern TEX$_{86}^{H}$ temperature is warmer (25.7°C) than the warmest SST of this area (21.0°C). Consequently, a seasonal shift of Thaumarchaeota production toward summer cannot alone explain such warm reconstructed temperatures. Global sediment calibrations fail in the reconstruction of local marine temperatures in this area.

Despite this apparent problem in reconstructions of absolute temperatures off Portugal with global calibrations, raw TEX$_{86}$ and $U_{37}^{K'}$ signals (Figures 2a and 2b) display a significant positive correlation for the last 70 kyr (Figure 3a, $R^2 = 0.79$). As $U_{37}^{K'}$ is interpreted as reflecting past annual mean SST, this high correlation with TEX$_{86}$ implies that TEX$_{86}$ should record a temperature signal proportional to SST variations.

Using the Bayesian spatially evolving calibration for TEX$_{86}$ based on annual mean SST [*Tierney and Tingley*, 2014, 2015], core top GDGT temperature is 20.2°C, close to the apparent summer SST for this area (21.0°C) (Figure 6). However, considering the mean ±4.4°C Bayesian calibration error for this reconstruction, the results are also comparable within errors with annual mean SST (18.0°C). This calibration takes into account regional effects since it gives larger weight to core top data up to 500 km away from MD95-2042 core site (12 core top sediments are more effective in our case: seven are located in the southern part of the Iberian Margin and in the Gulf of Cadiz [*Tierney and Tingley*, 2015]; cores IS-S1, IS-S2, and IS-S3 are in the Bay of Biscay [*Kim et al.*, 2010]; and cores 384B and 436B are in the westernmost Alboran Sea [*Nieto-Moreno et al.*, 2013]). The question is now to understand why global calibrations are not suitable for reconstructing realistic temperatures

on the Iberian Margin and which regional biases may be responsible for temperature overestimation via TEX_{86}^H reconstruction.

5.3. Possible Regional Biases Leading to SST-TEX_{86}^H Overestimation

A seasonal shift of Thaumarchaeota production toward the warm season is the first bias leading potentially to SST-TEX_{86}^H overestimation. Similar differences between TEX_{86}^H and $U_{37}^{K'}$ proxies were also reported in the neighboring Alboran Sea. They were interpreted as a shift in the season of production, with TEX_{86}^H reflecting mainly the warm summer season while $U_{37}^{K'}$ appeared to show annual mean SST [*Huguet et al.*, 2011; *Nieto-Moreno et al.*, 2013]. Such a shift of GDGT productivity toward the warmer season could contribute to a maximum increase of +3°C from annual mean SST on the Iberian Margin.

High nutrient concentration may also bring about a positive bias on TEX_{86}^H-derived temperature reconstructions since the difference between TEX_{86} temperature in particulate organic matter and in situ measured temperature increases with nitrate concentrations [*Turich et al.*, 2007]. On the Iberian Margin, a seasonality shift toward the warmer season would also correlate with a higher nutrient availability linked to summer upwelling [*Navarro and Ruiz*, 2006; *Rocha et al.*, 2013].

Terrigenous inputs—soil-derived iGDGTs—can potentially bias TEX_{86} temperature estimates [*Hopmans et al.*, 2004; *Weijers et al.*, 2006]. Even if core MD95-2042 is located offshore the Tagus River mouth, low BIT index values throughout the record (<0.06, not shown) suggest negligible riverine inputs of soil organic matter.

Allochthonous marine GDGTs may also bias the signal toward warmer temperatures. Indeed, a seasonal production of organic matter, coupled with a residence time in surface waters of 3 to 6 months allows its advection via high-speed surface currents in the North Atlantic Gyre. This could lead to a temperature bias of +2°C for the Iberian Margin area, according to simulations by *Rühlemann and Butzin* [2006]. However, alkenones are more prone to be laterally transported than GDGTs (Crenarchaeol) in shallow depth areas such as continental margins [*Mollenhauer et al.*, 2008]. Since our record based on alkenones does not exhibit unrealistic temperatures, this does not support their advection in this area, nor for GDGTs.

Community shifts in GDGT producers on the Iberian Margin may be responsible for unrealistic reconstructions using global calibrations. The calibrations are based on worldwide core tops integrating "global" dominant Thaumarchaeota species. But specific oceanographic settings, such as seasonal upwelling areas, could host archaeal species with different vital effects, thus leading to significant bias on TEX_{86} temperature reconstructions. Lipids from the epipelagic and upwelling/mesopelagic waters were differentiated based on the Caldarchaeol/Crenarchaeol ratio [*Turich et al.*, 2007]. Group 1 Crenarchaeota (recently renamed Thaumarchaeota [*Brochier-Armanet et al.*, 2008]) and a mix of Group II Euryarchaeota and Crenarchaeota represent the mesopelagic/upwelling and epipelagic end-members, respectively [*Turich et al.*, 2007] (Figure 2e). Euryarchaeota as a significant source of GDGTs to marine sediment could complicate the SST reconstructions based on these biomarkers [*Lincoln et al.*, 2014]. In upwelling areas, systematic bias toward higher temperatures for both core- and IPL-specific TEX_{86} values suggests subsurface in situ production of Archaea with a distinct relationship between lipid biosynthesis and temperature [*Basse et al.*, 2014], further supporting the contribution of endemic archaeal species with vital effect.

Based on the binary mix model outlined by *Turich et al.* [2007] (Figure 2e), the contribution of upwelling/mesopelagic Archaea is evaluated to range from 67% during the interglacial period to 28% during the mean glacial state and to 14% for Heinrich Stadials (Figure 2e). However, the variations of species contribution in core MD95-2042 (Caldarchaeol/Crenarchaeol ratio) are not clearly correlated to the difference between SST-TEX_{86}^H and SST-$U_{37}^{K'}$ ($n = 400$, $R^2 = 0.07$) (Figure 3e). Therefore, apparent variations of archaeal faunas through time are not responsible for variable bias on the TEX_{86} record. However, we cannot rule out the contribution of archaeal species/communities with different iGDGT distribution response to temperature than those commonly living at the surface. Our study site presents oceanographic similarities with the seasonal Mauritanian upwelling, where there is growing evidence for a major contribution of subsurface archaeal communities with differing temperature sensitivity [*Mollenhauer et al.*, 2015]. Furthermore, Mediterranean Overflow Waters are present between 500 and 1500 m depth on the Iberian Margin [*Zenk and Armi*, 1990; *Daniault et al.*, 1994; *Mazé et al.*, 1997; *van Aken*, 2000; *Ambar et al.*, 2002] and were deeper during glacial times [*Zahn et al.*, 1987; *Schönfeld and Zahn*, 2000; *Voelker et al.*, 2006]. The contribution

of deepwater dwelling Archaea from or similarly to the Mediterranean Sea, with different relationship to in situ temperature [*Kim et al.*, 2015], may also be worth considering. Deep archaeal community contribution to the sediment may be responsible for the warm bias as identified in the Mediterranean Sea, but with the TEX_{86} index still correlating to SST [*Kim et al.*, 2015]. Future studies combining geochemistry of GDGTs and archaeal microbiology are required on the Iberian Margin to decipher which hypotheses should be retained.

The various biases discussed above may explain the inability of global calibrations to reconstruct realistic annual mean SSTs on the Iberian Margin. However, the calibration put forward by *Tierney and Tingley* [2014, 2015] also takes into account a "regional effect" through its Bayesian spatially varying approach: in particular, more weight is given to surface sediment from the south of the Iberian Margin, whose TEX_{86} temperature reconstructions are higher than annual mean SST. The Bayesian calibration produces comparable results to $U_{37}^{k'}$ records (SST-TEX_{86} = $0.96 \pm 0.05 \times$ SST-$U_{37}^{k'}$ + 0.65 ± 0.72; R^2 = 0.79 and n = 400) (Figure 3c) and shows that a SST signal is recorded by TEX_{86} in core MD95-2042. A regional calibration is therefore required for the Iberian Margin to provide robust annual mean SST reconstructions, by counterbalancing regional biases affecting TEX_{86} reconstructions while using any global calibration.

5.4. Reconciling Data and Model

Figure 5 represents a summary of our biomarker results, as well as annual mean observations and model inputs, ROMS, and modeled annual production Tproxy outputs at MD95-2042 site for all three climate modes. This graph allows data-observation-model comparisons inside a particular climate state, as well as temperature differences between climate modes. Contrary to 0–200 m temperatures, a similar temperature amplitude between climate modes is reported for both biomarkers and the modeled surface signal (Figure 5). Whatever the considered item (organic proxy/observation/regional model/modeled annual surface production Tproxy), a systematic comparable temperature difference is observed. The difference between modern reconstruction and the last glacial state (Δ(PD-LGM)) is 5.5–7°C, while the temperature amplitude between the last glacial and Heinrich Stadial states (Δ(LGM-HS)) is 3–4°C (Figure 5). Except for annual surface production, these amplitudes are not found with other Tproxies. For instance, when the Tproxy with 0–200 m production is considered, whatever the season of production, the temperature amplitude Δ(PD-LGM) is lower: 3–4°C (Figure 5 and Table 2).

SST differences between climate modes are specific to a region, as opposed to a basin-wide scale. These thermal amplitudes differ for each region of the North Atlantic and cover a wide range of delta values, as seen both by data (e.g., between 0°C and 8°C for Δ(PD-LGM) for the North Atlantic area [*Waelbroeck et al.*, 2009; *Ho and Laepple*, 2015] or between 0 and 14°C for Δ(PD-HS) in eastern North Atlantic [*Patton et al.*, 2011]) and by modeling studies (e.g., between -2°C and 7°C for Δ(PI-LGM) for the North Atlantic domain [*Kageyama et al.*, 2013] or between -2°C and 10°C for Δ(LGM-HS) [*Prange et al.*, 2004; *Swingedouw et al.*, 2009]). Furthermore, due to varying oceanographic settings between climate modes, temperature amplitudes are even expected to be specific for the core site (Figures 7b1 and 7b2). Our modeling results for the Iberian Margin domain confirm the specificity of each location at this regional scale, as has recently been shown for past summer SST reconstructions at different time slices based on planktonic foraminifera assemblages [*Salgueiro et al.*, 2014]. This distinctive oceanic feature, the position-specific temperature amplitude between climate modes, supports the strength of our similar ΔT reconstructions by both $U_{37}^{k'}$ and TEX_{86} and Tproxy with annual surface production.

The easiest way to explain the same temperature amplitude between climate modes for both biomarkers and annual surface production Tproxy in a location with such regional specificities is the validity of the following three criteria, altogether: (i) the slopes of the linear calibrations are valid, (ii) the physics of the ocean (temperatures and circulations) are usable, and (iii) the Tproxy production hypothesis is correct.

5.5. A New Regional TEX_{86} Calibration

Similar temperature amplitudes between climate modes for data and the model suggest that the slopes of TEX global annual mean SST-based calibrations are correct for the Iberian Margin (Figure 4a and section 5.4). Therefore, reconstructions of absolute annual mean SST on the Iberian Margin are challenged by an unsuitable intercept of the linear equations. Here we propose a new preliminary regional calibration based on the following assumptions and statistics.

$U_{37}^{k'}$ SSTs from core MD95-2042 over the last 70 kyr are taken as reference data for annual mean SSTs to build the regional TEX_{86} calibration. Furthermore, the TEX_{86}^{H} calibration proposed by *Kim et al.* [2010] is the most commonly used calibration for temperature reconstructions based on iGDGTs [e.g., *Basse et al.*, 2014; *Hernández-Sánchez et al.*, 2014; *O'Brien et al.*, 2014; *Zhang et al.*, 2014; *Ho and Laepple*, 2015]. The slope of this calibration is valid for the reconstruction of annual mean SST in the Iberian Margin domain, since the linear regression between SST-TEX_{86}^{H} and SST-$U_{37}^{k'}$ has a slope of 1 (slope = 0.97 ± 0.05, R^2 = 0.79, n = 400) (Figure 3c). Therefore, we set the slope of the regional calibration as constant and equal to the slope of the global TEX_{86}^{H} calibration (68.4°C per TEX_{86}^{H} ratio unit) [*Kim et al.*, 2010]. The following linear equation can then be solved to propose a new intercept "β" to reconstruct present and paleo annual mean SST on the Iberian Margin:

$$\text{Paleo annual mean SST-}U_{37}^{k'} = 68.4 \times TEX_{86}^{H} + \beta \qquad (5)$$

with β equal to the mean of the differences between SST-$U_{37}^{k'}$ and $68.4 \times TEX_{86}^{H}$ (β = 33.0 ± 0.1°C, the standard error; n = 400). The calibration error is calculated as 2 standard deviations on the β intercept, which is equal to 2 standard deviations of the residuals between SST-TEX_{86}^{H} (this study's calibration) and SST-$U_{37}^{k'}$ for MD95-2042: ±2.5°C (Figure 3f). The calibration error is comparable to the global calibration error (±2.5°C [*Kim et al.*, 2010], Table 1) but may be underestimated because our regional calibration is based on several assumptions, each of which bears individual uncertainties. The first one is that the $U_{37}^{k'}$ temperature reflects the local annual mean SST for the last 70 kyr. The second assumption is that TEX_{86} records stable conditions from 70 ka B.P. to present. Similar temperature amplitudes both for organic proxies and for the model (section 5.4) provide strong evidence that both biomarkers record a SST signal and that conditions required for the application of our calibration were maintained for PD, LGM, and HS. However, these climate states may not encompass all climate conditions of the past 70 kyr: for instance, some sparse divergences exist between the two organic proxy reconstructions (Figure 6). An occasional shift in seasonality or archaeal community may disturb the validity of both the calibration slope and its applicability downcore, thereby compromising the ability to reconstruct reliable SSTs at all times. This type of complication is inherent to downcore calibrations, where environmental conditions are generally less constrained than in core top studies, for example. Therefore, to further evaluate our regional downcore calibration, we recommend the conduction of core top studies across the whole domain of the margin to build a regional core top calibration. In parallel, modern time series of alkenone and GDGT records, as well as species composition, should be generated for the Iberian Margin, to understand where, when, and which communities produce the exported signals and how they react to temperature.

The new regional "paleocalibration" equation (annual mean SST (°C) = $68.4 \times TEX_{86}^{H}$ + 33.0) provides an offset correction of −5.6°C to the global TEX_{86}^{H} calibration [*Kim et al.*, 2010] and gives similar temperature ranges for both TEX_{86}^{H} and $U_{37}^{k'}$ (Figure 4). This offset may suggest the contribution of different surface archaeal communities in the area. Indeed, a common slope with global calibrations indicates similar temperature sensitivity, but the different intercept suggests a species-dependent vital effect on initial GDGT distribution. Such offsets in calibration equations due to species-dependent vital effects are commonly described in geochemistry, e.g., for coral Sr/Ca thermometry [*Cardinal et al.*, 2001] or for planktonic foraminifera Mg/Ca thermometry [*Anand et al.*, 2003; *Skinner and Elderfield*, 2005]. Another explanation may be deeper archaeal production, as hypothesized in the Mauritanian upwelling and in the Mediterraean Sea [*Kim et al.*, 2015; *Mollenhauer et al.*, 2015]. Indeed, deep Mediterranean and Red Sea sediments align with a quasi *y* axis translation of the global linear calibration toward smaller temperatures [*Kim et al.*, 2015], in a way comparable to our regional calibration off Portugal (Figure 4). There is a need for genetic studies on Iberian Margin archaeal communities and for mesocosm experiments to confirm the prevalence of archaeal species with specific metabolic/thermodynamic GDGT production at different habitat depths.

SST-TEX_{86}^{H} reconstructions for core MD95-2042 using our new regional calibration give values comparable to reconstructions with the Bayesian spatially varying calibration [*Tierney and Tingley*, 2014, 2015] (Figure 6). However, we advise potential users that this regional TEX_{86} calibration is a preliminary tool, which requires further assessment through complementary studies (core top sediment calibration, GDGTs, and archaeal communities time series in the water column).

5.6. Iberian Margin Millennial-Scale Surface Variability

Both $TEX_{86}SST$ and $U^{k'}_{37}$ SST show in-phase warming at the transition between Dansgaard/Oeschger Stadials and Interstadials. Nevertheless, the shapes of DO Interstadials are different (Figure 6): while TEX^H_{86} reaches a thermal maximum at the beginning of the Greenland Interstadial (GI) and then decreases following a stepwise mode, as seen for the Greenland NGRIP $\delta^{18}O_{ice}$ record [Andersen et al., 2006; Svensson et al., 2006, 2008] (Figures 2a and S2a), $U^{k'}_{37}$ SST reaches the maximum value at the end of the interstadial and a sharp drop follows (Figure 2b). Similar behavior is observed during the last termination, especially during the Bolling/Allerod (DO 1) preceding the Younger Dryas, where the TEX^H_{86} signal mimics the behavior of the Greenland record (Figures 6 and S2a). Keeping in mind that Greenland $\delta^{18}O_{ice}$ is a nonlinear proxy for atmospheric temperature [Kindler et al., 2014], and considering that both biomarkers record SSTs off Portugal, we can tentatively interpret this contrasting behavior between organic proxies as being due to a progressive seasonal shift of alkenone production. Full interstadial conditions (at the beginning of a Greenland Interstadial) may favor alkenone production all year long. But surface conditions progressively became colder as the ensuing Greenland or Heinrich Stadial approached, as reported for Greenland climate variation [Andersen et al., 2006; Svensson et al., 2006, 2008] (Figure S2a). In response to this gradual cooling, coccolithophorid blooms may have progressively shifted toward the warmer season to adapt to the better living conditions (temperature, light, and nutrients). With the installation of full stadial conditions or Heinrich Stadials, the polar front was close to or reached the Iberian Margin [Bard et al., 1987; Eynaud et al., 2009], possibly preventing alkenone producers from blooming [Nishida, 1986; Sikes and Volkman, 1993], as seen by the synchronous and abrupt fall of both $U^{k'}_{37}$ SSTs and alkenone concentrations (Figures 2b and 2d). During Stadials, only small amounts of alkenone were produced, probably during summer when compared to absolute summer SSTs obtained with planktonic foraminifera assemblages [Cayre et al., 1999]. With the rapid retreat of the polar front at the onset of the Greenland Interstadial, alkenone producers benefited again from favorable blooming conditions. Meanwhile, Archaea, being more ubiquitous, could have thrived all year long during Stadials or Interstadials or at least could have kept the same seasonality. Therefore, Archaea may have recorded climate variations comparable to the Greenland NGRIP $\delta^{18}O_{ice}$ record.

Other differences in organic paleothermometer behaviors can also be seen throughout the LGM (between H2 and H1 events): TEX^H_{86} temperatures tend to decrease, while the $U^{k'}_{37}$ signal globally increases, as is the case for the Greenland record (Figure 6). During the LGM, a gradual change of archaeal exported production toward the colder season may be involved in the decrease of TEX^H_{86}-SSTs. Indeed, the summer upwelling is thought to have been more intense than at present, with higher primary productivity (Figure 2d) [Pailler and Bard, 2002]. At the end of this upwelling, chemoautotrophs such as Thaumarchaeota become more competitive for regenerated NH_4^+ [Ward, 1985] and may dwell preferentially during winter, as is observed in subpolar regions [Murray et al., 1998; Herfort et al., 2007; Manganelli et al., 2009]. The more intense the upwelling, the greater may be the archaeal population shift toward the cold season.

Moreover, during some intervals such as the late Holocene, the Bølling/Allerød, or Heinrich Stadial 6, TEX^H_{86} temperatures are still about 2°C higher than the $U^{k'}_{37}$ signal (Figure 6). These differences are within the calibration error but may reflect a contrasting behavior of the TEX_{86} index compared to the $U^{k'}_{37}$ index. During those intervals, deep-dwelling archaeal exported production may have been enhanced, positively biasing the TEX_{86}-based temperature record. Another explanation could be that archaeal production may occasionally have shifted toward the warmer season, as proposed for the Alboran Sea by Huguet et al. [2011].

6. Conclusions

We present two high-resolution continuous records of Iberian Margin annual mean SST based on $U^{k'}_{37}$ and TEX_{86} proxies for the past 70,000 years and a regional modeling effort to help interpret these signals by testing different production scenarios (season and depth).

The $U^{k'}_{37}$ index allows direct annual mean SST reconstruction using global calibration in core MD95-2042. Conversely, global TEX_{86} calibrations give much too warm temperature estimates for this area (+5.6°C). Regional biases hampering temperature reconstruction are mainly attributed to archaeal communities, which behave differently at this location than elsewhere in the ocean for unknown reasons. The comparison of GDGT temperature results with alkenones and modeled temperature proxies supports the production of a year long

surface TEX_{86} signal and allows us to establish a new regional calibration to reconstruct reliable past SSTs based on the TEX_{86} index for the Iberian Margin. Using TEX_{86} alone in this area would therefore give significantly erroneous results, and for this reason, TEX_{86} studies should be accompanied by at least a few alkenone comparisons.

This study with a dual approach combining organic geochemistry and regional modeling produces robust reconstitutions of annual mean SST for the last 70 kyr off Portugal. Similar millennial-scale variability patterns and quantitative records are observed for both $U_{37}^{k'}$ and TEX_{86} biomarkers, with the exception of some intervals during which regional biases may have occasionally changed (seasonality and archaeal communities).

Joint multiproxy and modeling studies have proved their ability to solve specific issues for biomarker paleothermometry, such as seasonality and depth of production of the temperature signal. Further study, involving the coupling of a biogeochemical model to the ocean physics model, could take into account more accurately the complexity of productivity for both alkenones and iGDGTs. The coupling of a sediment model could also give better quantification of biases due to degradation, resuspension, or reworking.

Note Added in Proof

Shortly after acceptance of our paper for publication, we became aware of a new relevant article [*Kim et al.*, 2016]. These authors studied suspended particulate matter and surface sediments off Portugal and measured GDGTs through organic geochemistry and performed genetic analyses of Thaumarchaeota. *Kim et al.* [2016] showed that a deep-water population residing in the Mediterranean Outflow Water (MOW) contributes significantly to the GDGT sedimentary signal, thus biasing positively TEX_{86}-based temperature reconstructions. These observations strengthen our observation and interpretation of the +5.6°C warm bias in TEX_{86}-temperatures measured downcore MD95-2042, as due to the contribution of endemic—possibly deep dwelling—archaeal communities bearing different GDGT distributions in relation to temperature.

References

Ambar, I., N. Serra, M. J. Brogueira, G. Cabeçadas, F. Abrantes, P. Freitas, C. Gonçalves, and N. Gonzalez (2002), Physical, chemical and sedimentological aspects of the Mediterranean outflow off Iberia, *Deep Sea Res., Part II*, *49*(19), 4163–4177, doi:10.1016/S0967-0645(02)00148-0.

Anand, P., H. Elderfield, and M. H. Conte (2003), Calibration of Mg/Ca thermometry in planktonic foraminifera from a sediment trap time series, *Paleoceanography*, *18*(2), 1050, doi:10.1029/2002KPA000846.

Andersen, K. K., et al. (2006), The Greenland Ice Core Chronology 2005, 15–42 ka. Part 1: Constructing the time scale, *Quat. Sci. Rev.*, *25*(23–24), 3246–3257, doi:10.1016/j.quascirev.2006.08.002.

Antonov, J. I., R. A. Locarnini, T. P. Boyer, A. V. Mishonov, and H. E. Garcia (2006), *World Ocean Atlas 2005, Volume 2: Salinity*, *NOAA Atlas NESDIS*, vol. 62, edited by S. Levitus, U.S. Gov. Print. Off., Washington, D. C.

Armstrong, E. M., and J. Vazquez-Cuervo (2001), A new global satellite-based sea surface temperature climatology, *Geophys. Res. Lett.*, *28*(22), 4199–4202, doi:10.1029/2001GL013316.

Aumont, O., and L. Bopp (2006), Globalizing results from ocean in situ iron fertilization studies, *Global Biogeochem. Cycles*, *20*, GB2017, doi:10.1029/2005GB002591.

Aumont, O., E. Maier-Reimer, S. Blain, and P. Monfray (2003), An ecosystem model of the global ocean including Fe, Si, P colimitations, *Global Biogeochem. Cycles*, *17*(2), 1060, doi:10.1029/2001GB001745.

Bard, E. (2001), Comparison of alkenone estimates with other paleotemperature proxies, *Geochem. Geophys. Geosyst.*, *2*(1), 1002, doi:10.1029/2000GC000050.

Bard, E., M. Arnold, P. Maurice, J. Duprat, J. Moyes, and J. Duplessy (1987), Retreat velocity of the North Atlantic polar front during the last deglaciation determined by ^{14}C accelerator mass spectrometry, *Nature*, *328*(6133), 791–794, doi:10.1038/328791a0.

Bard, E., F. Rostek, J. Turon, and S. Gendreau (2000), Hydrological impact of Heinrich events in the subtropical northeast Atlantic, *Science*, *289*(5483), 1321–1324, doi:10.1126/science.289.5483.1321.

Basse, A., C. Zhu, G. J. M. Versteegh, G. Fischer, K.-U. Hinrichs, and G. Mollenhauer (2014), Distribution of intact and core tetraether lipids in water column profiles of suspended particulate matter off Cape Blanc, NW Africa, *Org. Geochem.*, *72*, 1–13, doi:10.1016/j.orggeochem.2014.04.007.

Bassinot, F., and L. Labeyrie (1996), IMAGES MD 101 Brest-Marseille 29/05/95-11/07/95—A Coring Cruise of the R/V Marion Dufresne in the North Atlantic Ocean and Norwegian Sea, Les rapports de campagnes à la mer. Institut Français pour la Recherche et la Technologie Polaire., Plouzane, France.

Benthien, A., and P. J. Müller (2000), Anomalously low alkenone temperatures caused by lateral particle and sediment transport in the Malvinas Current region, western Argentine Basin, *Deep Sea Res., Part A*, *47*(12), 2369–2393, doi:10.1016/S0967-0637(00)00030-3.

Bogus, K. A., K. A. F. Zonneveld, D. Fischer, S. Kasten, G. Bohrmann, and G. J. M. Versteegh (2012), The effect of meter-scale lateral oxygen gradients at the sediment-water interface on selected organic matter based alteration, productivity and temperature proxies, *Biogeosciences*, *9*(4), 1553–1570, doi:10.5194/bg-9-1553-2012.

Bond, G., and R. Lotti (1995), Iceberg discharges into the North Atlantic on millennial time scales during the last glaciation, *Science*, *267*(5200), 1005–1010, doi:10.1126/science.267.5200.1005.

Bond, G., et al. (1992), Evidence for massive discharges of icebergs into the North Atlantic ocean during the last glacial period, *Nature*, *360*(6401), 245–249, doi:10.1038/360245a0.

Brassell, S., G. Eglinton, I. Marlowe, U. Pflaumann, and M. Sarnthein (1986), Molecular stratigraphy: A new tool for climatic assessment, *Nature*, *320*(6058), 129–133, doi:10.1038/320129a0.

Brochier-Armanet, C., B. Boussau, S. Gribaldo, and P. Forterre (2008), Mesophilic crenarchaeota: Proposal for a third archaeal phylum, the Thaumarchaeota, *Nat. Rev. Microbiol.*, *6*(3), 245–252, doi:10.1038/nrmicro1852.

Cardinal, D., B. Hamelin, E. Bard, and J. Patzold (2001), Sr/Ca, U/Ca and delta O-18 records in recent massive corals from Bermuda: Relationships with sea surface temperature, *Chem. Geol.*, *176*(1–4), 213–233, doi:10.1016/S0009-2541(00)00396-X.

Casey, K. S., and P. Cornillon (1999), A comparison of satellite and in situ-based sea surface temperature climatologies, *J. Clim.*, *12*(6), 1848–1863, doi:10.1175/1520-0442(1999)012<1848:ACOSAI>2.0.CO;2.

Casey, K. S., T. B. Brandon, P. Cornillon, and R. Evans (2010), The past, present, and future of the AVHRR Pathfinder SST program, in *Oceanography From Space*, edited by V. Barale, J. F. R. Gower, and L. Alberotanza, pp. 273–287, Springer, Dordrecht, Netherlands.

Castañeda, I. S., E. Schefuß, J. Pätzold, J. S. Sinninghe Damsté, S. Weldeab, and S. Schouten (2010), Millennial-scale sea surface temperature changes in the eastern Mediterranean (Nile River Delta region) over the last 27,000 years, *Paleoceanography*, *25*, PA1208, doi:10.1029/2009PA001740.

Cayre, O., Y. Lancelot, and E. Vincent (1999), Paleoceanographic reconstructions from planktonic foraminifera off the Iberian Margin: Temperature, salinity, and Heinrich events, *Paleoceanography*, *14*(3), 384–396, doi:10.1029/1998PA900027.

Conte, M. H., A. Thompson, D. Lesley, and R. P. Harris (1998), Genetic and physiological influences on the alkenone/alkenoate versus growth temperature relationship in *Emiliania huxleyi* and *Gephyrocapsa Oceanica*, *Geochim. Cosmochim. Acta*, *62*(1), 51–68, doi:10.1016/S0016-7037(97)00327-X.

Conte, M. H., M. Sicre, C. Ruhlemann, J. Weber, S. Schulte, D. Schulz-Bull, and T. Blanz (2006), Global temperature calibration of the alkenone unsaturation index (U-37(K')) in surface waters and comparison with surface sediments, *Geochem. Geophys. Geosyst.*, *7*, Q02005, doi:10.1029/2005GC001054.

Daniault, N., J. P. Mazé, and M. Arhan (1994), Circulation and mixing of Mediterranean water west of the Iberian Peninsula, *Deep Sea Res. Part Oceanogr. Res. Pap.*, *41*(11–12), 1685–1714, doi:10.1016/0967-0637(94)90068-X.

da Silva, A. M., C. C. Young, and S. Levitus (1994), *Atlas of Surface Marine Data 1994*, *NOAA Atlas NESDIS*, vol. 6, U.S. Department of Commerce, Washington, D. C.

de Leeuw, J. W., F. W. van der Meer, W. I. C. Rijpstra, and P. A. Schenck (1980), On the occurrence and structural identification of long chain unsaturated ketones and hydrocarbons in sediments, *Phys. Chem. Earth*, *12*, 211–217, doi:10.1016/0079-1946(79)90105-8.

Epstein, B. L., S. D'Hondt, J. G. Quinn, J. Zhang, and P. E. Hargraves (1998), An effect of dissolved nutrient concentrations on alkenone-based temperature estimates, *Paleoceanography*, *13*(2), 122–126, doi:10.1029/97PA03358.

Eynaud, F., et al. (2009), Position of the Polar Front along the western Iberian Margin during key cold episodes of the last 45 ka, *Geochem. Geophys. Geosyst.*, *10*, Q07U05, doi:10.1029/2009GC002398.

Fiuza, A. (1984), Hidrologica e Dinamica das Aguas Costeiras de Portugal, PhD thesis, Univ. de Lisboa, Lisbon.

Fiuza, A., M. Macedo, and R. Guerreiro (1982), Climatological space and time variation of the Portuguese coastal upwelling, *Oceanol. Acta*, *5*(1), 15–30.

Fiuza, A., M. Hamann, I. Ambar, G. del Rio, N. Gonzalez, and J. Cabanas (1998), Water masses and their circulation off western Iberia during May 1993, *Deep-Sea Res., Part A*, *45*(7), 1127–1160.

Gherardi, J., L. Labeyrie, J. McManus, R. Francois, L. Skinner, and E. Cortijo (2005), Evidence from the Northeastern Atlantic basin for variability in the rate of the meridional overturning circulation through the last deglaciation, *Earth Planet. Sci. Lett.*, *240*(3–4), 710–723, doi:10.1016/j.epsl.2005.09.061.

Gong, C., and D. J. Hollander (1999), Evidence for differential degradation of alkenones under contrasting bottom water oxygen conditions: Implication for paleotemperature reconstruction, *Geochim. Cosmochim. Acta*, *63*(3–4), 405–411, doi:10.1016/S0016-7037(98)00283-X.

Goni, M. A., M. P. Woodworth, H. L. Aceves, R. C. Thunell, E. Tappa, D. Black, F. Müller-Karger, Y. Astor, and R. Varela (2004), Generation, transport, and preservation of the alkenone-based $U_{37}^{K'}$, sea surface temperature index in the water column and sediments of the Cariaco Basin (Venezuela), *Global Biogeochem. Cycles*, *18*, GB2001, doi:10.1029/2003GB002132.

Grauel, A.-L., A. Leider, M.-L. S. Goudeau, I. A. Müller, S. M. Bernasconi, K.-U. Hinrichs, G. J. de Lange, K. A. F. Zonneveld, and G. J. M. Versteegh (2013), What do SST proxies really tell us? A high-resolution multiproxy ($U_{37}^{K'}$, TEX_{86}^{H} and foraminifera $\delta^{18}O$) study in the Gulf of Taranto, central Mediterranean Sea, *Quat. Sci. Rev.*, *73*, 115–131, doi:10.1016/j.quascirev.2013.05.007.

Heinrich, H. (1988), Origin and consequences of cyclic ice rafting in the Northeast Atlantic-Ocean during the past 130,000 years, *Quat. Res.*, *29*(2), 142–152, doi:10.1016/0033-5894(88)90057-9.

Herfort, L., S. Schouten, B. Abbas, M. J. W. Veldhuis, M. J. L. Coolen, C. Wuchter, J. P. Boon, G. J. Herndl, and J. S. Sinninghe Damsté (2007), Variations in spatial and temporal distribution of Archaea in the North Sea in relation to environmental variables, *FEMS Microbiol. Ecol.*, *62*, 242–257, doi:10.1111/j.1574-6941.2007.00397.x.

Hernández-Sánchez, M. T., E. M. S. Woodward, K. W. R. Taylor, G. M. Henderson, and R. D. Pancost (2014), Variations in GDGT distributions through the water column in the South East Atlantic Ocean, *Geochim. Cosmochim. Acta*, *132*, 337–348, doi:10.1016/j.gca.2014.02.009.

Herndl, G. J., T. Reinthaler, E. Teira, H. van Aken, C. Veth, A. Pernthaler, and J. Pernthaler (2005), Contribution of Archaea to total prokaryotic production in the deep Atlantic Ocean, *Appl. Environ. Microbiol.*, *71*(5), 2303–2309, doi:10.1128/AEM.71.5.2303-2309.2005.

Ho, S. L., and T. Laepple (2015), Glacial cooling as inferred from marine temperature proxies TEX_{86}^{H} and $U_{37}^{K'}$, *Earth Planet. Sci. Lett.*, *409*, 15–22, doi:10.1016/j.epsl.2014.10.033.

Hopmans, E., J. Weijers, E. Schefuss, L. Herfort, J. Damste, and S. Schouten (2004), A novel proxy for terrestrial organic matter in sediments based on branched and isoprenoid tetraether lipids, *Earth Planet. Sci. Lett.*, *224*(1–2), 107–116, doi:10.1016/j.epsl.2004.05.012.

Huguet, C., E. C. Hopmans, W. Febo-Ayala, D. H. Thompson, J. S. S. Damsté, and S. Schouten (2006a), An improved method to determine the absolute abundance of glycerol dibiphytanyl glycerol tetraether lipids, *Org. Geochem.*, *37*(9), 1036–1041, doi:10.1016/j.orggeochem.2006.05.008.

Huguet, C., J. Kim, J. Damste, and S. Schouten (2006b), Reconstruction of sea surface temperature variations in the Arabian Sea over the last 23 kyr using organic proxies (TEX_{86} and $U_{37}^{k'}$), *Paleoceanography*, *21*, PA3003, doi:10.1029/2005PA001215.

Huguet, C., A. Schimmelmann, R. Thunell, L. J. Lourens, J. S. Sinninghe Damsté, and S. Schouten (2007), A study of the TEX_{86} paleothermometer in the water column and sediments of the Santa Barbara Basin, California, *Paleoceanography*, *22*, PA3203, doi:10.1029/2006PA001310.

Huguet, C., J.-H. Kim, G. J. de Lange, J. S. Sinninghe Damsté, and S. Schouten (2009), Effects of long term oxic degradation on the $U_{37}^{k'}$, TEX_{86} and BIT organic proxies, *Org. Geochem.*, *40*(12), 1188–1194, doi:10.1016/j.orggeochem.2009.09.003.

Huguet, C., B. Martrat, J. O. Grimalt, J. S. Sinninghe Damsté, and S. Schouten (2011), Coherent millennial-scale patterns in $U_{37}^{k'}$ and TEX_{86}^{H} temperature records during the penultimate interglacial-to-glacial cycle in the western Mediterranean, *Paleoceanography*, *26*, PA2218, doi:10.1029/2010PA002048.

Ingalls, A. E., S. R. Shah, R. L. Hansman, L. I. Aluwihare, G. M. Santos, E. R. M. Druffel, and A. Pearson (2006), Quantifying archaeal community autotrophy in the mesopelagic ocean using natural radiocarbon, *Proc. Natl. Acad. Sci. U.S.A.*, *103*(17), 6442–6447, doi:10.1073/pnas.0510157103.

Jia, G., J. Zhang, J. Chen, P. Peng, and C. L. Zhang (2012), Archaeal tetraether lipids record subsurface water temperature in the South China Sea, *Org. Geochem.*, *50*, 68–77, doi:10.1016/j.orggeochem.2012.07.002.

Kageyama, M., J. Mignot, D. Swingedouw, C. Marzin, R. Alkama, and O. Marti (2009), Glacial climate sensitivity to different states of the Atlantic Meridional Overturning Circulation: Results from the IPSL model, *Clim. Past*, *5*(3), 551–570, doi:10.5194/cp-5-551-2009.

Kageyama, M., et al. (2013), Mid-Holocene and Last Glacial Maximum climate simulations with the IPSL model. Part II: Model-data comparisons, *Clim. Dyn.*, *40*(9–10), 2469–2495, doi:10.1007/s00382-012-1499-5.

Karner, M., E. DeLong, and D. Karl (2001), Archaeal dominance in the mesopelagic zone of the Pacific Ocean, *Nature*, *409*(6819), 507–510, doi:10.1038/35054051.

Kim, J.-H., S. Schouten, E. C. Hopmans, B. Donner, and J. S. Sinninghe Damsté (2008), Global sediment core-top calibration of the TEX$_{86}$ paleothermometer in the ocean, *Geochim. Cosmochim. Acta*, *72*(4), 1154–1173, doi:10.1016/j.gca.2007.12.010.

Kim, J.-H., C. Huguet, K. A. F. Zonneveld, G. J. M. Versteegh, W. Roeder, J. S. Sinninghe Damsté, and S. Schouten (2009), An experimental field study to test the stability of lipids used for the TEX$_{86}$ and palaeothermometers, *Geochim. Cosmochim. Acta*, *73*(10), 2888–2898, doi:10.1016/j.gca.2009.02.030.

Kim, J.-H., J. van der Meer, S. Schouten, P. Helmke, V. Willmott, F. Sangiorgi, N. Koç, E. C. Hopmans, and J. S. S. Damsté (2010), New indices and calibrations derived from the distribution of crenarchaeal isoprenoid tetraether lipids: Implications for past sea surface temperature reconstructions, *Geochim. Cosmochim. Acta*, *74*(16), 4639–4654, doi:10.1016/j.gca.2010.05.027.

Kim, J.-H., O. E. Romero, G. Lohmann, B. Donner, T. Laepple, E. Haam, and J. S. Sinninghe Damsté (2012), Pronounced subsurface cooling of North Atlantic waters off Northwest Africa during Dansgaard–Oeschger interstadials, *Earth Planet. Sci. Lett.*, *339–340*(0), 95–102, doi:10.1016/j.epsl.2012.05.018.

Kim, J.-H., et al. (2015), Influence of deep-water derived isoprenoid tetraether lipids on the paleothermometer in the Mediterranean Sea, *Geochim. Cosmochim. Acta*, *150*, 125–141, doi:10.1016/j.gca.2014.11.017.

Kim, J.-H., L. Villanueva, C. Zell, and J. S. Sinninghe Damsté (2016), Biological source and provenance of deep-water derived isoprenoid tetraether lipids along the Portuguese continental margin, *Geochim. Cosmochim. Acta*, *172*, 177–204, doi:10.1016/j.gca.2015.09.010.

Kindler, P., M. Guillevic, M. Baumgartner, J. Schwander, A. Landais, and M. Leuenberger (2014), Temperature reconstruction from 10 to 120 kyr b2k from the NGRIP ice core, *Clim. Past*, *10*(2), 887–902, doi:10.5194/cp-10-887-2014.

Konneke, M., A. E. Bernhard, J. R. de la Torre, C. B. Walker, J. B. Waterbury, and D. A. Stahl (2005), Isolation of an autotrophic ammonia-oxidizing marine archaeon, *Nature*, *437*(7058), 543–546, doi:10.1038/nature03911.

Lee, K. E., J.-H. Kim, I. Wilke, P. Helmke, and S. Schouten (2008), A study of the alkenone, TEX$_{86}$, and planktonic foraminifera in the Benguela Upwelling System: Implications for past sea surface temperature estimates, *Geochem. Geophys. Geosyst.*, *9*, Q10019, doi:10.1029/2008GC002056.

Leider, A., K.-U. Hinrichs, G. Mollenhauer, and G. J. Versteegh (2010), Core-top calibration of the lipid-based $U_{37}^{K'}$ and TEX$_{86}$ temperature proxies on the southern Italian shelf (SW Adriatic Sea, Gulf of Taranto), *Earth Planet. Sci. Lett.*, *300*(1–2), 112–124, doi:10.1016/j.epsl.2010.09.042.

Lengger, S. K., E. C. Hopmans, G.-J. Reichart, K. G. J. Nierop, J. S. Sinninghe Damsté, and S. Schouten (2012), Intact polar and core glycerol dibiphytanyl glycerol tetraether lipids in the Arabian Sea oxygen minimum zone. Part II: Selective preservation and degradation in sediments and consequences for the TEX$_{86}$, *Geochim. Cosmochim. Acta*, *98*, 244–258, doi:10.1016/j.gca.2012.05.003.

Lengger, S. K., M. Kraaij, R. Tjallingii, M. Baas, J.-B. Stuut, E. C. Hopmans, J. S. Sinninghe Damsté, and S. Schouten (2013), Differential degradation of intact polar and core glycerol dialkyl glycerol tetraether lipids upon post-depositional oxidation, *Org. Geochem.*, *65*, 83–93, doi:10.1016/j.orggeochem.2013.10.004.

Lengger, S. K., E. C. Hopmans, J. S. Sinninghe Damsté, and S. Schouten (2014), Impact of sedimentary degradation and deep water column production on GDGT abundance and distribution in surface sediments in the Arabian Sea: Implications for the TEX$_{86}$ paleothermometer, *Geochim. Cosmochim. Acta*, *142*, 386–399, doi:10.1016/j.gca.2014.07.013.

Li, D., M. Zhao, J. Tian, and L. Li (2013), Comparison and implication of TEX$_{86}$ and $U_{37}^{K'}$ temperature records over the last 356 kyr of ODP Site 1147 from the northern South China Sea, *Palaeogeogr. Palaeoclimatol. Palaeoecol.*, *376*, 213–223, doi:10.1016/j.palaeo.2013.02.031.

Lincoln, S. A., B. Wai, J. M. Eppley, M. J. Church, R. E. Summons, and E. F. DeLong (2014), Planktonic Euryarchaeota are a significant source of archaeal tetraether lipids in the ocean, *Proc. Natl. Acad. Sci. U.S.A.*, *111*(27), 9858–9863, doi:10.1073/pnas.1409439111.

Lipp, J. S., and K.-U. Hinrichs (2009), Structural diversity and fate of intact polar lipids in marine sediments, *Geochim. Cosmochim. Acta*, *73*(22), 6816–6833, doi:10.1016/j.gca.2009.08.003.

Lipp, J. S., Y. Morono, F. Inagaki, and K.-U. Hinrichs (2008), Significant contribution of Archaea to extant biomass in marine subsurface sediments, *Nature*, *454*(7207), 991–994, doi:10.1038/nature07174.

Liu, X., J. S. Lipp, and K.-U. Hinrichs (2011), Distribution of intact and core GDGTs in marine sediments, *Org. Geochem.*, *42*(4), 368–375, doi:10.1016/j.orggeochem.2011.02.003.

Liu, Z., M. Pagani, D. Zinniker, R. DeConto, M. Huber, H. Brinkhuis, S. R. Shah, R. M. Leckie, and A. Pearson (2009), Global cooling during the Eocene-Oligocene climate transition, *Science*, *323*(5918), 1187–1190, doi:10.1126/science.1166368.

Locarnini, R. A., A. V. Mishonov, J. I. Antonov, T. P. Boyer, and H. E. Garcia (2006), *World Ocean Atlas 2005, Volume 1: Temperature*, NOAA ATlas NESDIS, vol. 61, edited by S. Levitus, U.S. Gov. Print. Off., Washington, D. C.

Lopes dos Santos, R. A., M. Prange, I. S. Castañeda, E. Schefuß, S. Mulitza, M. Schulz, E. M. Niedermeyer, J. S. Sinninghe Damsté, and S. Schouten (2010), Glacial–interglacial variability in Atlantic meridional overturning circulation and thermocline adjustments in the tropical North Atlantic, *Earth Planet. Sci. Lett.*, *300*, 407–414, doi:10.1016/j.epsl.2010.10.030.

Lopes dos Santos, R. A., M. I. Spooner, T. T. Barrows, P. De Deckker, J. S. Sinninghe Damsté, and S. Schouten (2013), Comparison of organic ($U_{37}^{K'}$, TEX$_{86}^{H}$, LDI) and faunal proxies (foraminiferal assemblages) for reconstruction of late Quaternary sea surface temperature variability from offshore southeastern Australia, *Paleoceanography*, *28*, 377–387, doi:10.1002/palo.20035.

Lü, X., et al. (2014), Sources and distribution of isoprenoid glycerol dialkyl glycerol tetraethers (GDGTs) in sediments from the east coastal sea of China: Application of GDGT-based paleothermometry to a shallow marginal sea, *Org. Geochem.*, *75*, 24–35, doi:10.1016/j.orggeochem.2014.06.007.

Manganelli, M., F. Malfatti, T. J. Samo, B. G. Mitchell, H. Wang, and F. Azam (2009), Major role of microbes in carbon fluxes during austral winter in the southern drake passage, *Plos One*, *4*(9), e6941, doi:10.1371/journal.pone.0006941.

Mariotti, V., L. Bopp, A. Tagliabue, M. Kageyama, and D. Swingedouw (2012), Marine productivity response to Heinrich events: A model-data comparison, *Clim. Past*, *8*(5), 1581–1598, doi:10.5194/cp-8-1581-2012.

Marlowe, I., J. Green, A. Neal, S. Brassell, G. Eglinton, and P. Course (1984), Long chain (n-C$_{37}$–C$_{39}$) alkenones in the Prymnesiophyceae—Distribution of alkenones and other lipids and their taxonomic significance, *Br. Phycol. J.*, *19*(3), 203–216, doi:10.1080/00071618400650221.

Marti, O., et al. (2006), The new IPSL climate system model: IPSL-CM4, *IPSL Note Pô Modélisation*, *26*, 84.

Marti, O., et al. (2010), Key features of the IPSL ocean atmosphere model and its sensitivity to atmospheric resolution, *Clim. Dyn.*, *34*(1), 1–26, doi:10.1007/s00382-009-0640-6.

Martrat, B., J. Grimalt, N. Shackleton, L. de Abreu, M. Hutterli, and T. Stocker (2007), Four climate cycles of recurring deep and surface water destabilizations on the Iberian Margin, *Science*, *317*(5837), 502–507, doi:10.1126/science.1139994.

Martrat, B., P. Jimenez-Amat, R. Zahn, and J. O. Grimalt (2014), Similarities and dissimilarities between the last two deglaciations and interglaciations in the North Atlantic region, *Quat. Sci. Rev.*, *99*, 122–134, doi:10.1016/j.quascirev.2014.06.016.

Mazé, J. P., M. Arhan, and H. Mercier (1997), Volume budget of the eastern boundary layer off the Iberian Peninsula, *Deep Sea Res., Part A*, *44*(9–10), 1543–1574, doi:10.1016/S0967-0637(97)00038-1.

McClymont, E. L., R. S. Ganeshram, L. E. Pichevin, H. M. Talbot, B. E. van Dongen, R. C. Thunell, A. M. Haywood, J. S. Singarayer, and P. J. Valdes (2012), Sea-surface temperature records of Termination 1 in the Gulf of California: Challenges for seasonal and interannual analogues of tropical Pacific climate change, *Paleoceanography*, *27*, PA2202, doi:10.1029/2011PA002226.

McManus, J. F., R. Francois, J. M. Gherardi, L. D. Keigwin, and S. Brown-Leger (2004), Collapse and rapid resumption of Atlantic meridional circulation linked to deglacial climate changes, *Nature*, *428*(6985), 834–837, doi:10.1038/nature02494.

Ménot, G., and E. Bard (2012), A precise search for drastic temperature shifts of the past 40,000 years in southeastern Europe, *Paleoceanography*, *27*, PA2210, doi:10.1029/2012PA002291.

Mollenhauer, G., J. McManus, A. Benthien, P. Muller, and T. Eglinton (2006), Rapid lateral particle transport in the Argentine Basin: Molecular ^{14}C and $^{230}Th_{xs}$ evidence, *Deep Sea Res., Part A*, *53*(7), 1224–1243, doi:10.1016/j.dsr.2006.05.005.

Mollenhauer, G., M. Inthorn, T. Vogt, M. Zabel, J. Damste, and T. Eglinton (2007), Aging of marine organic matter during cross-shelf lateral transport in the Benguela upwelling system revealed by compound-specific radiocarbon dating, *Geochem. Geophys. Geosyst.*, *8*, Q09004, doi:10.1029/2007GC001603.

Mollenhauer, G., T. I. Eglinton, E. C. HopmanSd, and J. S. S. Damste (2008), A radiocarbon-based assessment of the preservation characteristics of crenarchaeol and alkenones from continental margin sediments, *Org. Geochem.*, *39*(8), 1039–1045, doi:10.1016/j.orggeochem.2008.02.006.

Mollenhauer, G., A. Basse, J.-H. Kim, J. S. Sinninghe Damsté, and G. Fischer (2015), A four-year record of $U_{37}^{K'}$- and TEX_{86}-derived sea surface temperature estimates from sinking particles in the filamentous upwelling region off Cape Blanc, Mauritania, *Deep Sea Res., Part A*, *97*, 67–79, doi:10.1016/j.dsr.2014.11.015.

Moreno, E., N. Thouveny, D. Delanghe, I. N. McCave, and N. J. Shackleton (2002), Climatic and oceanographic changes in the Northeast Atlantic reflected by magnetic properties of sediments deposited on the Portuguese Margin during the last 340 ka, *Earth Planet. Sci. Lett.*, *202*(2), 465–480, doi:10.1016/S0012-821X(02)00787-2.

Müller, P., G. Kirst, G. Ruhland, I. von Storch, and A. Rosell-Mele (1998), Calibration of the alkenone paleotemperature index $U_{37}^{K'}$ based on core-tops from the eastern South Atlantic and the global ocean (60°N-60°S), *Geochim. Cosmochim. Acta*, *62*(10), 1757–1772.

Murray, A. E., C. M. Preston, R. Massana, L. T. Taylor, A. Blakis, K. Wu, and E. F. DeLong (1998), Seasonal and spatial variability of bacterial and archaeal assemblages in the coastal waters near Anvers Island, Antarctica, *Appl. Environ. Microbiol.*, *64*(7), 2585–2595.

Nakanishi, T., M. Yamamoto, R. Tada, and H. Oda (2012a), Centennial-scale winter monsoon variability in the northern East China Sea during the Holocene, *J. Quat. Sci.*, *27*(9), 956–963, doi:10.1002/jqs.2589.

Nakanishi, T., M. Yamamoto, T. Irino, and R. Tada (2012b), Distribution of glycerol dialkyl glycerol tetraethers, alkenones and polyunsaturated fatty acids in suspended particulate organic matter in the East China Sea, *J. Oceanogr.*, *68*(6), 959–970, doi:10.1007/s10872-012-0146-4.

National Geophysical Data Center (2001), N. NOAA, U.S. Department of Commerce ETOPO2, Global 2 Arc-minute Ocean Depth and Land Elevation from the US National Geophysical Data Center (NGDC).

Navarro, G., and J. Ruiz (2006), Spatial and temporal variability of phytoplankton in the Gulf of Cádiz through remote sensing images, *Deep Sea Res., Part II*, *53*(11–13), 1241–1260, doi:10.1016/j.dsr2.2006.04.014.

Nieto-Moreno, V., F. Martínez-Ruiz, V. Willmott, J. García-Orellana, P. Masqué, and J. S. Sinninghe Damsté (2013), Climate conditions in the westernmost Mediterranean over the last two millennia: An integrated biomarker approach, *Org. Geochem.*, *55*, 1–10, doi:10.1016/j.orggeochem.2012.11.001.

Nishida, S. (1986), Nannoplankton flora in the southern ocean, with special reference to siliceous varieties, *Mem. Natl. Inst. Polar Res. Spec. Issue Jpn.*, *40*, 56–68.

Nolasco, R., A. C. Pires, N. Cordeiro, B. Le Cann, and J. Dubert (2013), A high-resolution modeling study of the Western Iberian Margin mean and seasonal upper ocean circulation, *Ocean Dyn.*, *63*(9–10), 1041–1062, doi:10.1007/s10236-013-0647-8.

O'Brien, C. L., G. L. Foster, M. A. Martinez-Boti, R. Abell, J. W. B. Rae, and R. D. Pancost (2014), High sea surface temperatures in tropical warm pools during the Pliocene, *Nat. Geosci.*, *7*(8), 607–612.

Ohkouchi, N., T. Eglinton, L. Keigwin, and J. Hayes (2002), Spatial and temporal offsets between proxy records in a sediment drift, *Science*, *298*(5596), 1224–1227, doi:10.1126/science.1075287.

Pailler, D., and E. Bard (2002), High frequency palaeoceanographic changes during the past 140000 yr recorded by the organic matter in sediments of the Iberian Margin, *Palaeogeogr. Palaeoclimatol. Palaeoecol.*, *181*(4), 431–452, doi:10.1016/S0031-0182(01)00444-8.

Patton, G. M., P. A. Martin, A. Voelker, and E. Salgueiro (2011), Multiproxy comparison of oceanographic temperature during Heinrich Events in the eastern subtropical Atlantic, *Earth Planet. Sci. Lett.*, *310*(1–2), 45–58, doi:10.1016/j.epsl.2011.07.028.

Peliz, A., J. Dubert, D. B. Haidvogel, and B. Le Cann (2003), Generation and unstable evolution of a density-driven Eastern Poleward Current: The Iberian Poleward Current, *J. Geophys. Res.*, *108*(C8), 3268, doi:10.1029/2002JC001443.

Peliz, A., J. Dubert, A. Santos, P. Oliveira, and B. Le Cann (2005), Winter upper ocean circulation in the Western Iberian Basin—Fronts, eddies and poleward flows: An overview, *Deep-Sea Res., Part A*, *52*(4), 621–646, doi:10.1016/j.dsar.2004.11.005.

Penven, P., L. Debreu, P. Marchesiello, and J. C. McWilliams (2006), Evaluation and application of the ROMS 1-way embedding procedure to the central California upwelling system, *Ocean Model.*, *12*(1–2), 157–187, doi:16/j.ocemod.2005.05.002.

Pires, A. C., R. Nolasco, and J. Dubert (2013), On the origin of summer upwelled waters on the Western Iberian Margin, *J. Coastal Res.*, *65*, 1993–1998, doi:10.2112/SI65-337.1.

Pires, A. C., R. Nolasco, A. Rocha, A. M. Ramos, and J. Dubert (2014), Global climate models as forcing for regional ocean modeling: A sensitivity study in the Iberian Basin (Eastern North Atlantic), *Clim. Dyn.*, *43*(3–4), 1083–1102, doi:10.1007/s00382-014-2151-3.

Prahl, F., L. Muehlhausen, and D. Zahnle (1988), Further evaluation of long-chain alkenones as indicators of paleoceanographic conditions, *Geochim. Cosmochim. Acta*, *52*(9), 2303–2310, doi:10.1016/0016-7037(88)90132-9.

Prahl, F., G. Delange, M. Lyle, and M. Sparrow (1989), Post-depositional stability of long-chain alkenones under contrasting redox conditions, *Nature*, *341*(6241), 434–437, doi:10.1038/341434a0.

Prahl, F. G., and S. G. Wakeham (1987), Calibration of unsaturation patterns in long-chain ketone compositions for palaeotemperature assessment, *Nature*, *330*(6146), 367–369, doi:10.1038/330367a0.

Prahl, F. G., R. B. Collier, J. Dymond, M. Lyle, and M. A. Sparrow (1993), A biomarker perspective on prymnesiophyte productivity in the northeast Pacific Ocean, *Deep Sea Res., Part A*, 40(10), 2061–2076, doi:10.1016/0967-0637(93)90045-5.

Prahl, F. G., C. H. Pilskaln, and M. A. Sparrow (2001), Seasonal record for alkenones in sedimentary particles from the Gulf of Maine, *Deep-Sea Res., Part A*, 48(2), 515–528, doi:10.1016/S0967-0637(00)00057-1.

Prahl, F. G., G. V. Wolfe, and M. A. Sparrow (2003), Physiological impacts on alkenone paleothermometry, *Paleoceanography*, 18(2), 1025, doi:10.1029/2002PA000803.

Prahl, F. G., B. N. Popp, D. M. Karl, and M. A. Sparrow (2005), Ecology and biogeochemistry of alkenone production at station ALOHA, *Deep Sea Res., Part A*, 52(5), 699–719, doi:10.1016/j.dsr.2004.12.001.

Prahl, F. G., J.-F. Rontani, N. Zabeti, S. E. Walinsky, and M. A. Sparrow (2010), Systematic pattern in $U_{37}^{k'}$—Temperature residuals for surface sediments from high latitude and other oceanographic settings, *Geochim. Cosmochim. Acta*, 74(1), 131–143, doi:10.1016/j.gca.2009.09.027.

Prange, M., G. Lohmann, V. Romanova, and M. Butzin (2004), Modelling tempo-spatial signatures of Heinrich Events: Influence of the climatic background state, *Quat. Sci. Rev.*, 23(5–6), 521–527, doi:10.1016/j.quascirev.2003.11.004.

Rocha, C., N. Cordeiro, R. Nolasco, and J. Dubert (2013), Numerical modelling of the phytoplankton patterns in an upwelling event off the NW Iberian Margin, *J. Coastal Res.*, 65, 117–122, doi:10.2112/SI65-021.1.

Rodrigues, T., A. H. L. Voelker, J. O. Grimalt, F. Abrantes, and F. Naughton (2011), Iberian Margin sea surface temperature during MIS 15 to 9 (580–300 ka): Glacial suborbital variability versus interglacial stability, *Paleoceanography*, 26, PA1204, doi:10.1029/2010PA001927.

Rommerskirchen, F., T. Condon, G. Mollenhauer, L. Dupont, and E. Schefuss (2011), Miocene to Pliocene development of surface and subsurface temperatures in the Benguela Current system, *Paleoceanography*, 26, PA3216, doi:10.1029/2010PA002074.

Rontani, J.-F., and S. G. Wakeham (2008), Alteration of alkenone unsaturation ratio with depth in the Black Sea: Potential roles of stereomutation and aerobic biodegradation, *Org. Geochem.*, 39(9), 1259–1268, doi:10.1016/j.orggeochem.2008.06.002.

Rontani, J.-F., P. Bonin, F. G. Prahl, I. D. Jameson, and J. K. Volkman (2006), Experimental and field evidence for thiyl radical-induced stereomutation of alkenones and other lipids in sediments and seawater, *Org. Geochem.*, 37(11), 1489–1504, doi:10.1016/j.orggeochem.2006.06.021.

Rontani, J.-F., I. Jameson, S. Christodoulou, and J. K. Volkman (2007), Free radical oxidation (autoxidation) of alkenones and other lipids in cells of Emiliania huxleyi, *Phytochemistry*, 68(6), 913–924, doi:10.1016/j.phytochem.2006.12.013.

Rontani, J.-F., R. Harji, S. Guasco, F. G. Prahl, J. K. Volkman, N. B. Bhosle, and P. Bonin (2008), Degradation of alkenones by aerobic hetero-trophic bacteria: Selective or not?, *Org. Geochem.*, 39(1), 34–51, doi:10.1016/j.orggeochem.2007.10.003.

Rontani, J.-F., N. Zabeti, and S. G. Wakeham (2009), The fate of marine lipids: Biotic vs. abiotic degradation of particulate sterols and alkenones in the Northwestern Mediterranean Sea, *Mar. Chem.*, 113(1–2), 9–18, doi:10.1016/j.marchem.2008.11.001.

Rosell-Melé, A., G. Eglinton, U. Pflaumann, and M. Sarnthein (1995), Atlantic core-top calibration of the U37K index as a sea-surface palaeotemperature indicator, *Geochim. Cosmochim. Acta*, 59(15), 3099–3107, doi:10.1016/0016-7037(95)00199-A.

Rosell-Melé, A., et al. (2001), Precision of the current methods to measure the alkenone proxy $U_{37}^{k'}$ and absolute alkenone abundance in sediments: Results of an interlaboratory comparison study, *Geochem. Geophys. Geosyst.*, 2(7), 1046, doi:10.1029/2000GC000141.

Rühlemann, C., and M. Butzin (2006), Alkenone temperature anomalies in the Brazil-Malvinas Confluence area caused by lateral advection of suspended particulate material, *Geochem. Geophys. Geosyst.*, 7, Q10015, doi:10.1029/2006GC001251.

Salgueiro, E., et al. (2014), Past circulation along the western Iberian Margin: A time slice vision from the Last Glacial to the Holocene, *Quat. Sci. Rev.*, 106, 316–329, doi:10.1016/j.quascirev.2014.09.001.

Sanchez, R., and P. Relvas (2003), Spring-summer climatological circulation in the upper layer in the region of Cape St. Vincent, Southwest Portugal, *ICES J. Mar. Sci.*, 60(6), 1232–1250, doi:10.1016/S1054-3139(03)00137-1.

Sanchi, L., G. Ménot, and E. Bard (2013), An automated purification method for archaeal and bacterial tetraethers in soils and sediments, *Org. Geochem.*, 54, 83–90, doi:10.1016/j.orggeochem.2012.10.005.

Savitzky, A., and M. J. E. Golay (1964), Smoothing and differentiation of data by simplified least squares procedures, *Anal. Chem.*, 36(8), 1627–1639, doi:10.1021/ac60214a047.

Sawada, K., N. Handa, and T. Nakatsuka (1998), Production and transport of long-chain alkenones and alkyl alkenoates in a sea water column in the northwestern Pacific off central Japan, *Mar. Chem.*, 59(3–4), 219–234, doi:10.1016/S0304-4203(97)00074-1.

Schneider, B., G. Leduc, and W. Park (2010), Disentangling seasonal signals in Holocene climate trends by satellite-model-proxy integration, *Paleoceanography*, 25, PA4217, doi:10.1029/2009PA001893.

Schönfeld, J., and R. Zahn (2000), Late Glacial to Holocene history of the Mediterranean Outflow. Evidence from benthic foraminiferal assemblages and stable isotopes at the Portuguese margin, *Palaeogeogr. Palaeoclimatol. Palaeoecol.*, 159(1–2), 85–111, doi:10.1016/S0031-0182(00)00035-3.

Schouten, S., E. Hopmans, E. Schefuss, and J. Damste (2002), Distributional variations in marine crenarchaeotal membrane lipids: A new tool for reconstructing ancient sea water temperatures?, *Earth Planet. Sci. Lett.*, 204(1–2), 265–274, doi:10.1016/S0012-821X(02)00979-2.

Schouten, S., E. C. Hopmans, and J. S. Sinninghe Damsté (2004), The effect of maturity and depositional redox conditions on archaeal tetraether lipid palaeothermometry, *Org. Geochem.*, 35(5), 567–571, doi:10.1016/j.orggeochem.2004.01.012.

Schouten, S., A. Forster, F. E. Panoto, and J. S. Sinninghe Damsté (2007), Towards calibration of the TEX$_{86}$ palaeothermometer for tropical sea surface temperatures in ancient greenhouse worlds, *Org. Geochem.*, 38(9), 1537–1546, doi:10.1016/j.orggeochem.2007.05.014.

Schouten, S., et al. (2009), An interlaboratory study of TEX$_{86}$ and BIT analysis using high-performance liquid chromatography–mass spectrometry, *Geochem. Geophys. Geosyst.*, 10, Q03012, doi:10.1029/2008GC002221.

Schouten, S., et al. (2013a), An interlaboratory study of TEX$_{86}$ and BIT analysis of sediments, extracts, and standard mixtures, *Geochem. Geophys. Geosyst.*, 14, 5263–5285, doi:10.1002/2013GC004904.

Schouten, S., E. C. Hopmans, and J. S. Sinninghe Damsté (2013b), The organic geochemistry of glycerol dialkyl glycerol tetraether lipids: A review, *Org. Geochem.*, 54, 19–61, doi:10.1016/j.orggeochem.2012.09.006.

Seki, O., D. N. Schmidt, S. Schouten, E. C. Hopmans, J. S. Sinninghe Damsté, and R. D. Pancost (2012), Paleoceanographic changes in the Eastern Equatorial Pacific over the last 10 Myr, *Paleoceanography*, 27, PA3224, doi:10.1029/2011PA002158.

Shaari, H. b., M. Yamamoto, and T. Irino (2013), Enhanced upwelling in the eastern equatorial Pacific at the last five glacial terminations, *Palaeogeogr. Palaeoclimatol. Palaeoecol.*, 386, 8–15, doi:10.1016/j.palaeo.2013.03.022.

Shackleton, N. J., M. A. Hall, and E. Vincent (2000), Phase relationships between millennial-scale events 64,000-24,000 years ago, *Paleoceanography*, 15(6), 565–569, doi:10.1029/2000PA000513.

Shah, S. R., G. Mollenhauer, N. Ohkouchi, T. I. Eglinton, and A. Pearson (2008), Origins of archaeal tetraether lipids in sediments: Insights from radiocarbon analysis, *Geochim. Cosmochim. Acta*, 72(18), 4577–4594, doi:10.1016/j.gca.2008.06.021.

Shchepetkin, A. F., and J. C. McWilliams (2005), The regional oceanic modeling system (ROMS): A split-explicit, free-surface, topography-following-coordinate oceanic model, *Ocean Model.*, *9*(4), 347–404, doi:16/j.ocemod.2004.08.002.

Shintani, T., M. Yamamoto, and M.-T. Chen (2011), Paleoenvironmental changes in the northern South China Sea over the past 28,000 years: A study of TEX$_{86}$-derived sea surface temperatures and terrestrial biomarkers, *J. Asian Earth Sci.*, *40*(6), 1221–1229, doi:10.1016/j.jseaes.2010.09.013.

Sicre, M.-A., G. Siani, D. Genty, N. Kallel, and L. Essallami (2013), Seemingly divergent sea surface temperature proxy records in the central Mediterranean during the last deglaciation, *Clim. Past*, *9*(3), 1375–1383, doi:10.5194/cp-9-1375-2013.

Sikes, E., and J. Volkman (1993), Calibration of alkenone unsaturation ratios (U-37(K')) for paleotemperature estimation in cold waters, *Geochim. Cosmochim. Acta*, *57*(8), 1883–1889.

Sikes, E. L., J. K. Volkman, L. G. Robertson, and J. J. Pichon (1997), Alkenones and alkenes in surface waters and sediments of the Southern Ocean: Implications for paleotemperature estimation in polar regions, *Geochim. Cosmochim. Acta*, *61*(7), 1495–1505, doi:10.1016/S0016-7037(97)00017-3.

Sinninghe Damsté, J. S., W. I. C. Rijpstra, E. C. Hopmans, F. G. Prahl, S. G. Wakeham, and S. Schouten (2002), Distribution of membrane lipids of planktonic Crenarchaeota in the Arabian Sea, *Appl. Environ. Microbiol.*, *68*(6), 2997–3002, doi:10.1128/AEM.68.6.2997-3002.2002.

Skinner, L. C., and H. Elderfield (2005), Constraining ecological and biological bias in planktonic foraminiferal Mg/Ca and $\delta^{18}O_{cc}$: A multispecies approach to proxy calibration testing, *Paleoceanography*, *20*, PA1015, doi:10.1029/2004PA001058.

Slutz, R. J., S. J. Lubker, J. D. Hiscox, S. D. Woodruff, R. L. Jenne, P. M. Steurer, and J. D. Elms (1985), *Comprehensive Ocean–Atmosphere Data Set: Release 1*, Clim. Res. Program, Boulder, Colo.

Smith, M., P. De Deckker, J. Rogers, J. Brocks, J. Hope, S. Schmidt, R. L. dos Santos, and S. Schouten (2013), Comparison of U$_{37}^{k'}$, TEX$_{86}^{H}$ and LDI temperature proxies for reconstruction of south-east Australian ocean temperatures, *Org. Geochem.*, *64*, 94–104, doi:10.1016/j.orggeochem.2013.08.015.

Sonzogni, C., E. Bard, F. Rostek, R. Lafont, A. Rosell-Mele, and G. Eglinton (1997), Core-top calibration of the alkenone index vs sea surface temperature in the Indian Ocean, *Deep Sea Res. Part II*, *44*(6–7), 1445–1460, doi:10.1016/S0967-0645(97)00010-6.

Studer, A. S., A. Martínez-Garcia, S. L. Jaccard, F. E. Girault, D. M. Sigman, and G. H. Haug (2012), Enhanced stratification and seasonality in the Subarctic Pacific upon Northern Hemisphere Glaciation—New evidence from diatom-bound nitrogen isotopes, alkenones and archaeal tetraethers, *Earth Planet. Sci. Lett.*, *351–352*, 84–94, doi:10.1016/j.epsl.2012.07.029.

Sun, M.-Y., and S. G. Wakeham (1994), Molecular evidence for degradation and preservation of organic matter in the anoxic Black Sea Basin, *Geochim. Cosmochim. Acta*, *58*(16), 3395–3406, doi:10.1016/0016-7037(94)90094-9.

Svensson, A., et al. (2006), The Greenland Ice Core Chronology 2005, 15–42 ka. Part 2: Comparison to other records, *Quat. Sci. Rev.*, *25*(23–24), 3258–3267, doi:10.1016/j.quascirev.2006.08.003.

Svensson, A., et al. (2008), A 60 000 year Greenland stratigraphic ice core chronology, *Clim. Past*, *4*(1), 47–57, doi:10.5194/cp-4-47-2008.

Swingedouw, D., J. Mignot, P. Braconnot, E. Mosquet, M. Kageyama, and R. Alkama (2009), Impact of freshwater release in the North Atlantic under different climate conditions in an OAGCM, *J. Clim.*, *22*(23), 6377–6403, doi:10.1175/2009JCLI3028.1.

Ternois, Y., M. A. Sicre, A. Boireau, J. C. Marty, and J. C. Miquel (1996), Production pattern of alkenones in the Mediterranean Sea, *Geophys. Res. Lett.*, *23*(22), 3171–3174, doi:10.1029/96GL02910.

Ternois, Y., M. A. Sicre, A. Boireau, M. H. Conte, and G. Eglinton (1997), Evaluation of long-chain alkenones as paleo-temperature indicators in the Mediterranean Sea, *Deep-Sea Res., Part A*, *44*(2), 271–286, doi:10.1016/S0967-0637(97)89915-3.

Ternois, Y., K. Kawamura, N. Ohkouchi, and L. Keigwin (2000), Alkenone sea surface temperature in the Okhotsk Sea for the last 15 kyr, *Geochem. J.*, *34*(4), 283–293.

Thouveny, N., J. Carcaillet, E. Moreno, G. Leduc, and D. Nerini (2004), Geomagnetic moment variation and paleomagnetic excursions since 400 kyr BP: A stacked record from sedimentary sequences of the Portuguese margin, *Earth Planet. Sci. Lett.*, *219*(3–4), 377–396, doi:10.1016/S0012-821X(03)00701-5.

Tierney, J. E., and M. P. Tingley (2014), A Bayesian, spatially-varying calibration model for the TEX$_{86}$ proxy, *Geochim. Cosmochim. Acta*, *127*, 83–106, doi:10.1016/j.gca.2013.11.026.

Tierney, J. E., and M. P. Tingley (2015), A TEX$_{86}$ surface sediment database and extended Bayesian calibration, *Sci. Data*, *2*, doi:10.1038/sdata.2015.29.

Turich, C., K. Freeman, M. Bruns, M. Conte, A. Jones, and S. Wakeham (2007), Lipids of marine Archaea: Patterns and provenance in the water-column and sediments, *Geochim. Cosmochim. Acta*, *71*(13), 3272–3291, doi:10.1016/j.gca.2007.04.013.

Turich, C., S. Schouten, R. C. Thunell, R. Varela, Y. Astor, and S. G. Wakeham (2013), Comparison of TEX$_{86}$ and temperature proxies in sinking particles in the Cariaco Basin, *Deep Sea Res., Part A*, *78*, 115–133, doi:10.1016/j.dsr.2013.02.008.

van Aken, H. M. (2000), The hydrography of the mid-latitude Northeast Atlantic Ocean. II: The intermediate water masses, *Deep Sea Res., Part A*, *47*(5), 789–824, doi:10.1016/S0967-0637(99)00112-0.

Versteegh, G. J. M., R. Riegman, J. W. de Leeuw, and J. H. F. Jansen (2001), U$_{37}^{k'}$ values for *Isochrysis galbana* as a function of culture temperature, light intensity and nutrient concentrations, *Org. Geochem.*, *32*(6), 785–794, doi:10.1016/S0146-6380(01)00041-9.

Voelker, A., S. Lebreiro, J. Schonfeld, I. Cacho, H. Erlenkeuser, and F. Abrantes (2006), Mediterranean outflow strengthening during northern hemisphere coolings: A salt source for the glacial Atlantic?, *Earth Planet. Sci. Lett.*, *245*(1–2), 39–55, doi:10.1016/j.epsl.2006.03.014.

Voelker, A. H. L., and L. de Abreu (2011), A review of abrupt climate change events in the Northeastern Atlantic Ocean (Iberian Margin): Latitudinal, longitudinal, and vertical gradients, in *Abrupt Climate Change: Mechanisms, Patterns, and Impacts*, vol. 193, edited by H. Rashid, L. Polyak, and E. Mosley-Thompson, pp. 15–37, AGU, Washington, D. C.

Volkman, J., G. Eglinton, E. Corner, and T. Forsberg (1980), Long-chain alkenes and alkenones in the marine coccolithophorid *Emiliania huxleyi*, *Phytochemistry*, *19*(12), 2619–2622, doi:10.1016/S0031-9422(00)83930-8.

Volkman, J., S. Barrett, S. Blackburn, and E. Sikes (1995), Alkenones in *Gephyrocapsa Oceanica*—Implications for studies of paleoclimate, *Geochim. Cosmochim. Acta*, *59*(3), 513–520, doi:10.1016/0016-7037(95)00325-T.

Waelbroeck, C., et al. (2009), Constraints on the magnitude and patterns of ocean cooling at the Last Glacial Maximum, *Nat. Geosci.*, *2*(2), 127–132, doi:10.1038/NGEO411.

Ward, B. B. (1985), Light and substrate concentration relationships with marine ammonium assimilation and oxidation rates, *Mar. Chem.*, *16*(4), 301–316, doi:10.1016/0304-4203(85)90052-0.

Weijers, J., S. Schouten, O. Spaargaren, and J. S. Sinninghe Damsté (2006), Occurrence and distribution of tetraether membrane lipids in soils: Implications for the use of the TEX$_{86}$ proxy and the BIT index, *Org. Geochem.*, *37*(12), 1680–1693, doi:10.1016/j.orggeochem.2006.07.018.

Weijers, J. W. H., K. L. H. Lim, A. Aquilina, J. S. S. Damste, and R. D. Pancost (2011), Biogeochemical controls on glycerol dialkyl glycerol tetraether lipid distributions in sediments characterized by diffusive methane flux, *Geochem. Geophys. Geosyst.*, *12*, Q10010, doi:10.1029/2011GC003724.

Wuchter, C., S. Schouten, M. J. L. Coolen, and J. S. S. Damste (2004), Temperature-dependent variation in the distribution of tetraether membrane lipids of marine Crenarchaeota: Implications for TEX_{86} paleothermometry, *Paleoceanography*, *19*, PA4028, doi:10.1029/2004PA001041.

Wuchter, C., S. Schouten, S. G. Wakeham, and J. S. S. Damste (2005), Temporal and spatial variation in tetraether membrane lipids of marine Crenarchaeota in particulate organic matter: Implications for TEX_{86} paleothermometry, *Paleoceanography*, *20*(3), doi:10.1029/2004PA001110.

Wuchter, C., et al. (2006), Archaeal nitrification in the ocean, *Proc. Natl. Acad. Sci. U.S.A.*, *103*(33), 12,317–12,322, doi:10.1073/pnas.0600756103.

Yamamoto, M., A. Shimamoto, T. Fukuhara, Y. Tanaka, and J. Ishizaka (2012), Glycerol dialkyl glycerol tetraethers and TEX_{86} index in sinking particles in the western North Pacific, *Org. Geochem.*, *53*, 52–62, doi:10.1016/j.orggeochem.2012.04.010.

Zabeti, N., P. Bonin, J. K. Volkman, I. D. Jameson, S. Guasco, and J.-F. Rontani (2010), Potential alteration of $U_{37}^{k'}$ paleothermometer due to selective degradation of alkenones by marine bacteria isolated from the haptophyte Emiliania huxleyi, *FEMS Microbiol. Ecol.*, *73*(1), 83–94, doi:10.1111/j.1574-6941.2010.00885.x.

Zahn, R., M. Sarnthein, and H. Erlenkeuser (1987), Benthic isotope evidence for changes of the Mediterranean outflow during the Late Quaternary, *Paleoceanography*, *2*(6), 543–559, doi:10.1029/PA002i006p00543.

Zenk, W., and L. Armi (1990), The complex spreading pattern of mediterranean water off the portuguese continental-slope, *Deep-Sea Res., Part A*, *37*(12), 1805–1823, doi:10.1016/0198-0149(90)90079-B.

Zhang, J., Y. Bai, S. Xu, F. Lei, and G. Jia (2013), Alkenone and tetraether lipids reflect different seasonal seawater temperatures in the coastal northern South China Sea, *Org. Geochem.*, *58*, 115–120, doi:10.1016/j.orggeochem.2013.02.012.

Zhang, Y. G., M. Pagani, and Z. Liu (2014), A 12-million-year temperature history of the tropical pacific ocean, *Science*, *344*(6179), 84–87, doi:10.1126/science.1246172.

Erratum

In the originally published version of this article, Table 1 contained errors at the bottom part of the 2nd and 6th columns. These have since been corrected and this version may be considered the authoritative version of record.